Excitonic Coherent Emission Process in Semiconductors

TAKASHI KURODA

Doctor's thesis submitted to Hokkaido University, 1994

Excitonic Coherent Emission Process in Semiconductors

Takashi Kuroda

Department of Physics, Faculty of Science
Hokkaido University

Electronic Coherent Emission Process in Semiconductors

Takashi Kuroda

Department of Physics, Faculty of Science
Hokkaido University

Excitonic Coherent Emission Process in Semiconductors

Takashi Kuroda
Department of Physics, Faculty of Science
Hokkaido University

Abstract

Coherent emission process of excitons in a layered compound GaSe, and in $ZnSe/ZnS_{0.18}Se_{0.82}$ multiple quantum wells has been directly observed for the first time, by means of two independent newly-developed methods; time-resolved Brewster-angle reflectance (TRBR) spectroscopy and time-resolved four-wave-mixing (TRFWM) spectroscopy.

In TRBR measurement, we have succeeded in observing a distinct free-induction-decay of coherently-driven polarization, with an oscillatory behavior due to finely split exciton levels. An analysis on the basis of a simple model provides key information on the dynamical phase relaxation process.

The result of the TRFWM measurement gives the comprehensive treatment of two dephasing processes; destructive interference due to static inhomogeneous broadening, and dynamical homogeneous phase relaxation. An analysis of TRFWM intensity enables one to exactly determine the homogeneous phase relaxation time.

Finally, we show that a comparison between the coherent emission signal measured by TRBR or TRFWM, and third-order nonlinear correlation profile observed by time-integrated FWM measurement enables one to make distinction between which of quantum- or classical interference effect causes the beat feature seen in the coherent emission signal.

Contents

I. Introduction

It is well known that a resonantly excited atom acquires a polarization, oscillating at the natural frequency and eventually decays away. This basic emission process, named coherent emission, is experimentally observed by measuring the temporal evolution of emitted intensity after short pulse excitation. In solids, however, atoms are densely packed, so that absorption and emission are strongly influenced by the interaction imposed on the elementary excitation with other degrees of freedom, which disturbs the phase ordering of the polarization within a few picoseconds. Because the dephasing time is very short in such media, direct experimental investigation of the coherent emission process has not been reported up to now.

In the present work, we study the coherent emission process of excitons in semiconductors with subpicosecond time resolution, by means of two independent methods newly developed, i. e., time-resolved Brewster-angle reflectance spectroscopy (TRBR) and time-resolved four-wave-mixing spectroscopy (TRFWM). By adopting these methods, the nonresonant contribution to the signal is extremely reduced, so that a clear and background-free coherent-polarization-related signal can be obtained. The signal shows a free-induction-decay (FID) and a quantum beat due to coherently driven excitonic polarization.

The constitution of this thesis is as follows: In Section II, we show the results of TRBR experiment for a layered compound GaSe and ZnSe/$ZnS_{0.18}Se_{0.82}$ multiple quantum wells (MQW's). For both samples, the TRBR signal shows a clear coherent emission signals; a decay feature reflecting the phase relaxation with an oscillatory structure due to split exciton lines. In Section III, we discuss the temporal profile of FWM signals of excitons in GaSe. In this sample, the spectral widths due to the inhomogeneous and homogeneous broadenings of the relevant exciton are almost same. Thus the FWM signal shows the intermediate nature of photon-echo type and exponential form for FID. In Section IV, we discuss the physical origin of the temporal oscillation seen in the coherent emission signals. Comparison between the time-integrated FWM signals and coherent emission reveals which of quantum- or classical interference effect causes the observed temporal oscillatory profile. A brief conclusion is given in Sec. V.

II. Linear coherent emission process studied by time-resolved Brewster-angle reflectance spectroscopy

Transient spectroscopy has been widely used for investigating coherence property of excitons in semiconductors. One of the important techniques is to observe a free-induction-decay signal, reflecting the superradiated coherent emission process. Since observations of this signal have been mostly demonstrated with utilizing a time-of-flight measurement, i. e., measurement of the temporal shape of a transmitted pulse, the results are often discussed from the view point of the coherent light propagation phenomenon.[1] In order to investigate directly the coherent emission process with neglecting a propagation effect, it may be effective to observe FID signals under reflectance geometry. However, a reflected signal is dominated by nonresonant component contributing to the reflectance, and thereby, a coherently emitted signal is masked by this nonresonant component. This disadvantage can be circumvented by adopting a Brewster-angle reflectance (BR) geometry.

Recently, we have reported that reflectance spectra at Brewster-angle of incidence show a distinct excitonic profile, with a great reduction of the nonresonant contribution to the reflectance.[2,3] By applying this configuration to transient spectroscopy,[4-8] it may be possible to obtain a clear and background-free coherent-polarization-related signal.

In this section, we report a time-resolved observation of the BR pulse (TRBR) for a layered compound GaSe and $ZnSe/ZnS_{0.18}Se_{0.82}$ MQW's. The signal provides a clear coherent emission; FID of the coherently driven polarization, and an oscillatory feature due to the interference between the split exciton states involved in the present sample.

II-1. Theoretical consideration

First, we briefly argue theoretically the temporal shape of a BR pulse. In the linear regime, the temporal shape of an output pulse is given by

$$E_{out}(t) = \int_0^\infty d\tau\, G(\tau)\, E_{in}(t - \tau)\,, \qquad (1)$$

where E_{in}, and $E_{out}(\tau)$ are the temporal form of the input and output pulses, respectively, $G(\tau)$ represents a response function which is given by Fourier transform of the frequency dispersion of the relevant optical process $\tilde{G}(\omega)$. We consider the reflectance geometry for p polarization with Brewster-angle of incidence. In this case $\tilde{G}(\omega)$ is given by the well-known Fresnel's formula. The incident angle is defined as $\arctan(n)$, where n is the

refractive index in the absence of the relevant exciton resonance. Assuming for simplicity that the dielectric function in question can be described in terms of an oscillator model, $G(\tau)$ can be derived as

$$G(\tau) \propto \theta(\tau) \exp\left[(-i\omega_0 - T_2^{-1})\tau\right], \qquad (2)$$

where T_2 is the phase relaxation time, ω_0 is the exciton energy in frequency, and $\theta(\tau)$ is a step function. Thus, the BR pulse is simply expressed by the exponentially decaying response of phase relaxation, with a freely-scattered component eliminated. The derivation of Eq. 2 is presented in Appendix A.

II-2. Experimental

a. Samples

Experiments were performed on two kinds of samples; GaSe and ZnSe/ZnSSe MQW's. The sample of GaSe used was of good quality and prepared from a single crystal which was grown by Bridgeman method. Flat and clean surfaces for reflectance measurement were obtained by cleaving a crystal with the planes perpendicular to the c-axis. The sample was thick enough (more than 0.5 mm) so as to neglect the multiple reflection effects. However, it is remarked that stacking faults parallel to the layers were easily seen. For MQW samples, two kinds of $ZnSe/ZnS_xSe_{1-x}$ ($x = 0.18$) MQW's were used, which consist of 210 periods of a 19-A-thick ZnSe well and a 19-A-thick ZnSSe barrier, and 80 periods of a 50-A ZnSe and a 50-A ZnSSe. Those were grown on (001) GaAs substrates by atmospheric metalorganic vapor-phase epitaxy at a growth temperature of 515 °C. Growth interruption of 30 s was inserted at each heterointerface.

b. Experimental procedure

In the present experiment, the temporal shape of a reflected pulse was measured with subpicosecond time resolution. The experimental setup is shown in Fig. 2-1. The resonant pulses with the beam divergence of $< 1°$ impinged on a sample at the Brewster-angle of incidence; the incident angle was set so as to be a Brewster-angle calculated with the known refractive index of GaSe or ZnSe in the transparent energy region just below the exciton resonance. (~70° for GaSe, and ~ 68° for ZnSe). To resolve the BR pulse temporally, the cross-correlation measurement was utilized, that is, the reflected beam

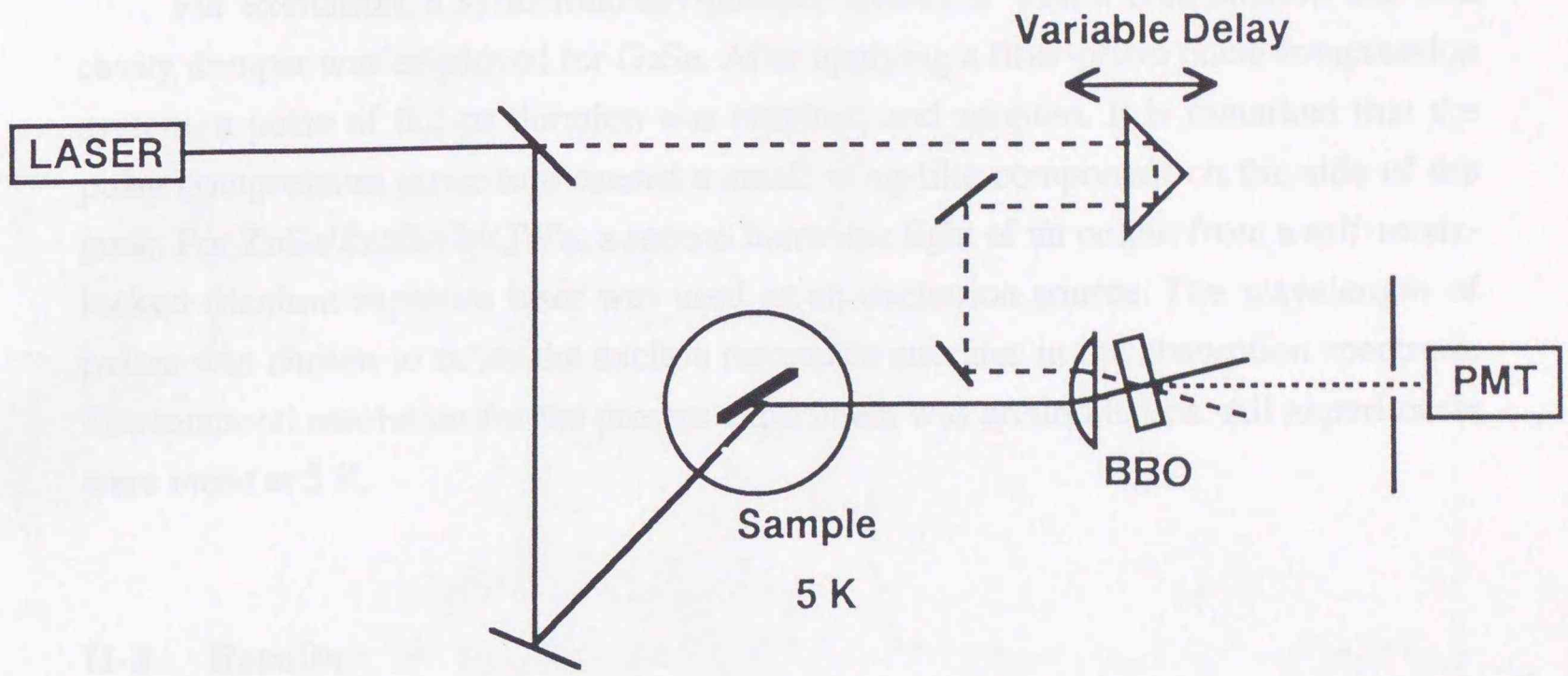

FIG. 2-1. Experimental setup of time-resolved Brewster-angle reflectance spectroscopy

was mixed with a reference pulse, devided from the same excitation beam, in a BBO crystal, and the intensity of an output sum-frequency-generated (SFG) light was measured as a function of mutual delay time. Since SFG intensity displays the magnitude of temporal superposition between the reference short pulse and the signal, the intensity as a function of the delay time of the reference pulse gives the time-resolved intensity of the BR pulse with subpicosecond time resolution.

For excitation, a synchronously-pumped dye-laser with a combination use of a cavity dumper was employed for GaSe. After applying a fiber-prism pulse compression system, a pulse of 0.2-ps duration was obtained and adopted. It is remarked that the pulse compression procedure caused a small wing-like component on the side of the peak. For ZnSe/ZnSSe MQW's, a second harmonic light of an output from a self-mode-locked titanium sapphire laser was used as an excitation source. The wavelength of pulses was chosen to cover the exciton resonance energies in the absorption spectrum. The temporal resolution for the present experiment was around 0.3 ps. All experiments were made at 5 K.

II-3. Results

a. GaSe

In Fig. 2-2, stationary reflectance spectra at Brewster-angle incidence are shown. The reflectivity for a p-polarized beam shows that a very strong sharp profile manifests itself, the peak energy of which coincides with the excitonic resonance energy. Small fluctuations observed in the nonresonant energy region should be caused by an interference profile due to random stacking faults involved in GaSe. It was found that the reflectance spectra of the excitonic resonance was almost similar to that in the absorption which was observed in a thin film sample cleaved from the same crystal.

In Fig. 2-3, results of TRBR are presented. For an s-polarized beam, the observed temporal form of a reflected pulse is seen to be symmetric, which was almost identical to the auto-correlation trace of an excitation pulse. On the other hand, for a p-polarized beam, the signal exhibits a distinct decay profile and an oscillatory structure is found to be superimposed on the signal. A sharp dip profile seen at $t = 0$ should arise from an interference between two components of reflected beams; nonresonant contribution which is extremely reduced by adopting Brewster-angle of incidence but still remains due to a small divergence of the incident angle, and resonant contribution. The phase of two beams is different to each other, and thereby, a *coherent dip* may appear: Similar behavior has been reported very recently in Ref. [9].

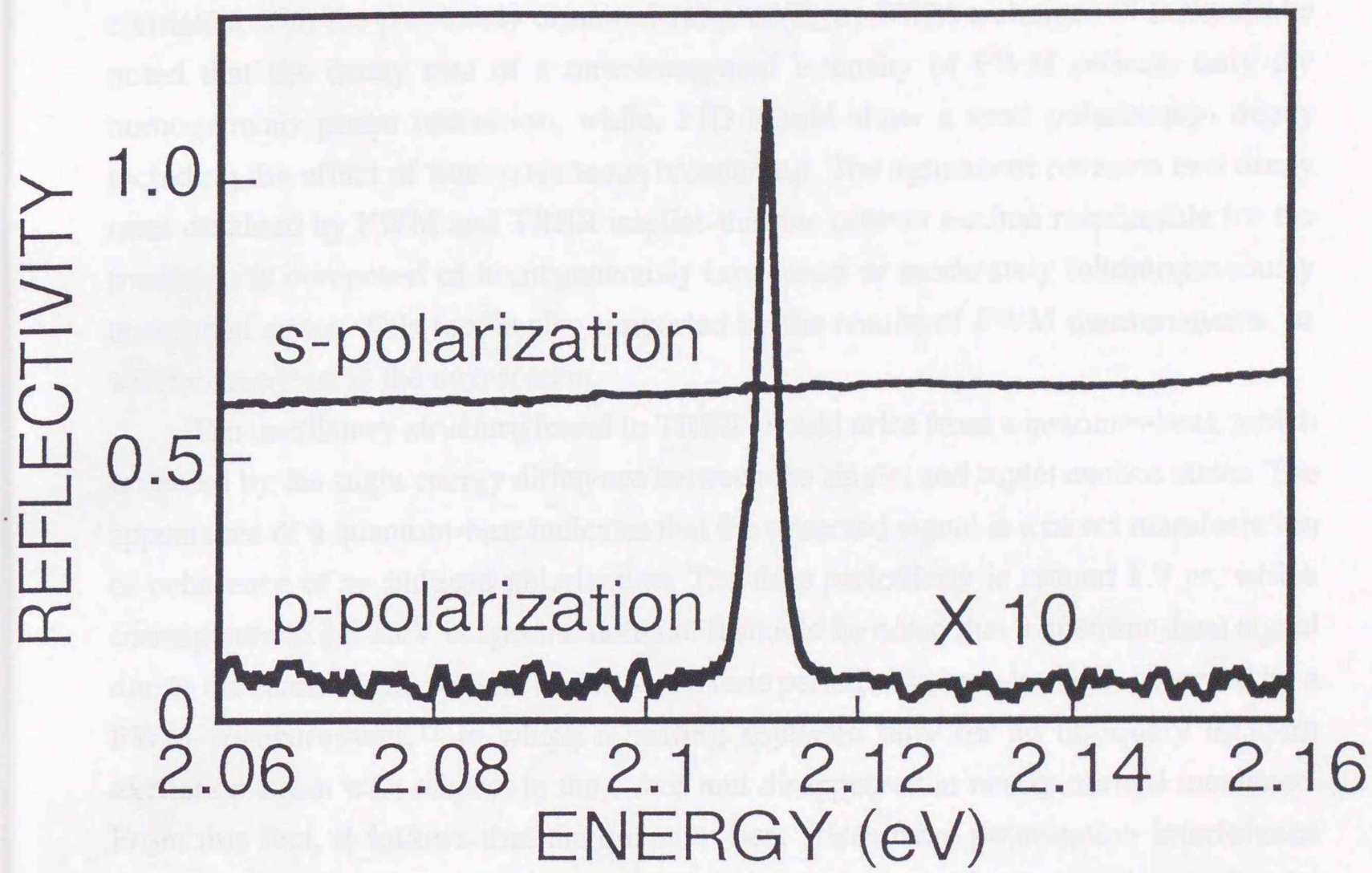

FIG. 2-2. Stationary reflectance spectra of GaSe at Brewster-angle of incidence.

The decay profile is seen to obey a single exponential curve. This should be a FID of a coherent polarization, which can be observed clearly and directly by means of the present reflectance technique. The characteristic time of the decay is estimated as ~ 2.5 ps, which may correspond to a dephasing time, T_2, of ~ 5 ps. This quantity is quite consistent with the previously observed value of T_2 by FWM technique.[10] It should be noted that the decay rate of a time-integrated intensity of FWM reflects only the homogeneous phase relaxation, while, FID would show a total polarization decay including the effect of inhomogeneous broadening. The agreement between two decay rates obtained by FWM and TRBR implies that the present exciton responsible for the transition is composed of homogeneously broadened or moderately inhomogeneously broadened states. This fact is also supported by the results of FWM measurements, as will be described in the next section.

The oscillatory structure found in TRBR should arise from a quantum-beat, which is caused by the slight energy difference between the singlet and triplet exciton states. The appearance of a quantum-beat indicates that the observed signal is a direct manifestation of coherence of an induced polarization. The time periodicity is around 1.9 ps, which corresponds to 2.1 meV in spectral domain. It should be noted that a quantum-beat signal due to the same origin, with an almost equal time periodicity, has also been observed by a FWM measurement,[11] in which a beating appeared only for an obliquely incident excitation beam with respect to the c-axis and disappeared at nearly-normal incidence. From this fact, it follows that the quantum-beat arises from polarization interference between split singlet and triplet excitons, both of which are optically allowed for the configuration of oblique incidence.

In Fig. 2-4, the dependence of the TRBR signal on the excitation intensity is presented. It is seen that the signal varies drastically with changing the excitation density. At very low excitation densities, an unusual slow rise of a signal was found. This interesting behavior will be considered in Discussions. Aside from this, the decay time, or T_2, was observed to decrease with increasing the density, which may be ascribed to the change of the incoherent scattering rate between excitons.

In Fig. 2-5, the spectra of reflected pulses corresponding to Fig. 2-4 are shown. Excitonic resonant profile consists of two lines corresponding to the singlet and triplet exciton states. The energy splitting, 1.8 meV, is in reasonable agreement with the periodicity of the quantum-beat in TRBR. Furthermore, the spectral fine structure is found to be less clear at higher intensities, where fast phase relaxation due to incoherent scattering induces a broad linewidth which screens the split spectra. The corresponding behavior in time domain is also found in TRBR: for higher densities the beat profile become less clear, which is masked by a fast decay component of FID.

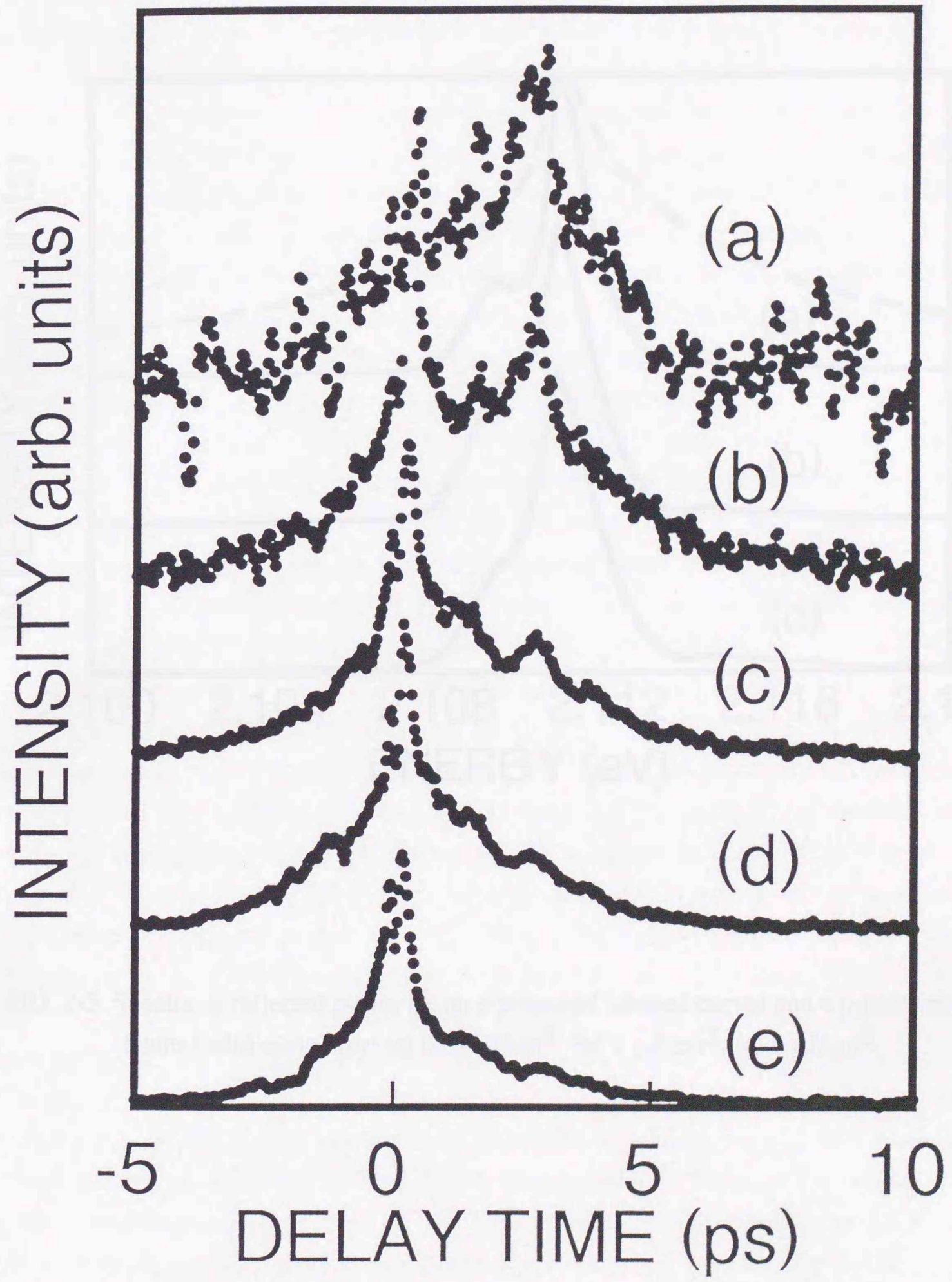

FIG. 2-4. Intensity dependence of the temporal shape of reflected pulses: (a) 0.05 $\mu J/cm^2$ (1×10^8 excitons/cm^2), (b) 0.25 $\mu J/cm^2$, (c) 1 $\mu J/cm^2$, (d) 2.5 $\mu J/cm^2$, (e) 5 $\mu J/cm^2$.

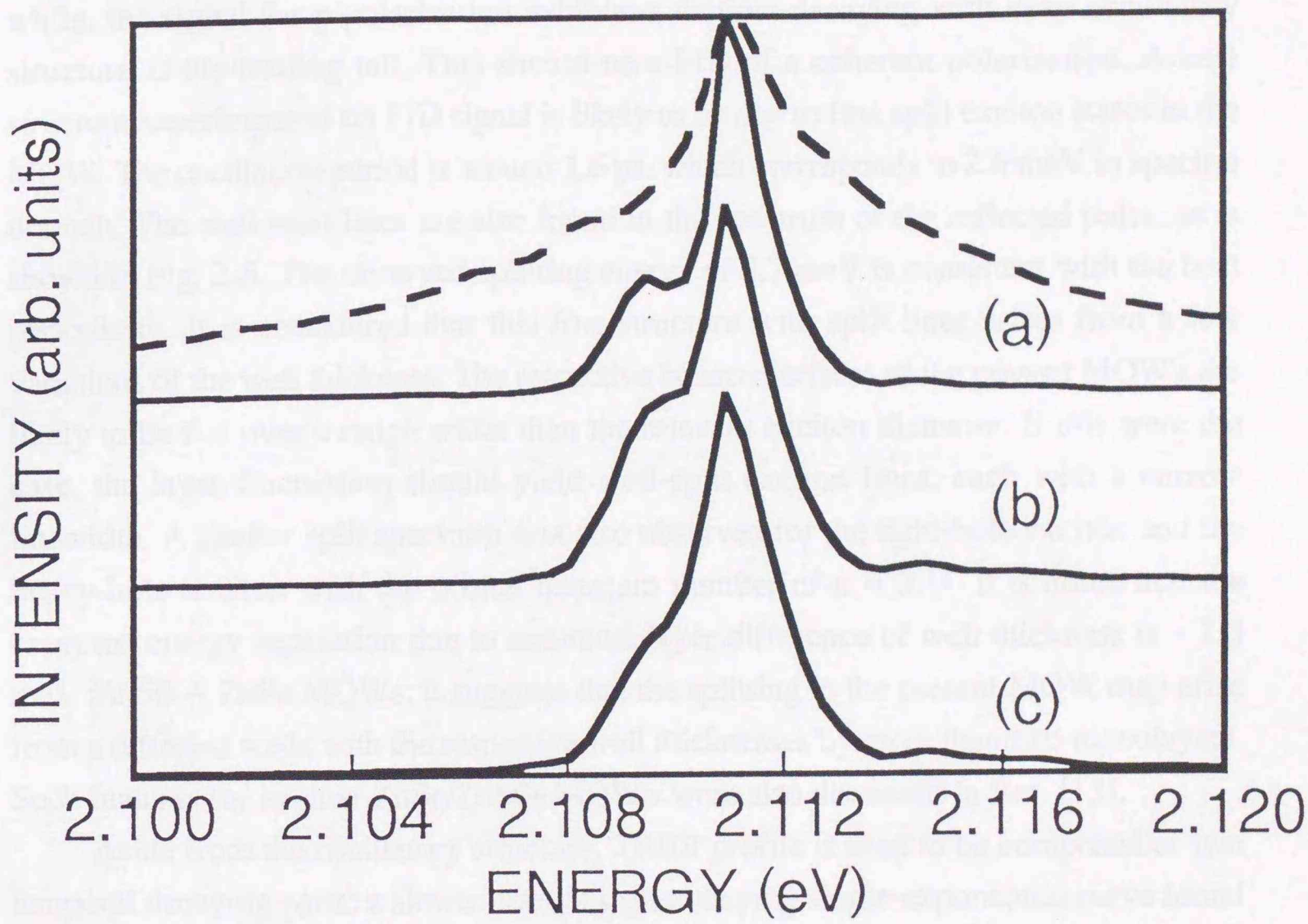

FIG. 2-5. Spectra of reflected pulses for an s-polarized (dashed curve) and a p-polarized beam (solid curve) for: (a) 0.25 $\mu J/cm^2$, (b) 1 $\mu J/cm^2$, (c) 5 $\mu J/cm^2$.

b. ZnSe/ZnSSe multiple quantum wells

In Fig. 2-6, a typical TRBR profile for the 50 A/50 A MQW is presented. Similarly to the results for GaSe, the temporal form for s polarization is seen to be symmetric, while, the signal for p polarization exhibits a distinct decaying with deep oscillatory structure at the trailing tail. This should be a FID of a coherent polarization. A beat structure superimposed on FID signal is likely to be due to fine split exciton states in the MQW. The oscillation period is around 1.6 ps, which corresponds to 2.6 meV in spectral domain. The well-split lines are also found in the spectrum of the reflected pulse, as is shown in Fig. 2-8. The observed splitting energy of 2.7 meV is consistent with the beat periodicity. It is considered that this fine structure with split lines arises from a few variations of the well thickness: The respective heterointerfaces of the present MQW's are likely to be flat over a range wider than the relevant exciton diameter. If this were the case, the layer fluctuation should yield well-split exciton lines, each with a narrow linewidth. A similar split spectrum was also observed for the light-hole exciton and the heavy-hole exciton with the orbital quantum number of n = 2.[12] It is noted that the expected energy separation due to one-monolayer difference of well thickness is ~ 1.3 meV for 50-A ZnSe MQWs. It suggests that the splitting in the present MQW may arise from a different wells with the respective well thicknesses by more than two monolayers. Such features for another ZnSe/ZnSSe MQW's were also discussed in Ref. [13].

Aside from the oscillatory structure, TRBR profile is seen to be composed of two temporal decaying parts; a slower decaying part obeying single-exponential curve found at the earlier stage, and a very fast decaying part at the later stage. The former should reflect the homogeneous phase relaxation, while for the latter, the origin is not clear to us at present. It is noted that such a rapid change of the decay rate is not expected by introducing a simple inhomogeneous broadening: A Gaussian distribution of exciton energies would only provide a quadratic curve in a log-plot of FID intensity. However, the FID signal decays as a single-exponential curve until the signal decreases by two orders of magnitude. This fact shows that the destructive interference effect caused by an inhomogeneous broadening does not greatly contribute to the FID process. Thus, the relevant exciton line is considered to be essentially homogeneously broadened. With the decay rate defined as a time constant Γ of the exponential curve for an FID signal, the phase relaxation time T_2' is given by $2/\Gamma$. Thus, a value of T_2' is extracted as 2.8 ± 0.3 ps. This value is consistent with the result of a FWM measurement, which has been performed on the same sample.[14]

Following the above procedure, the dependence of the homogeneous linewidth Γ on the excitation density is plotted in Fig. 2-9. It is found that the phase relaxation rate

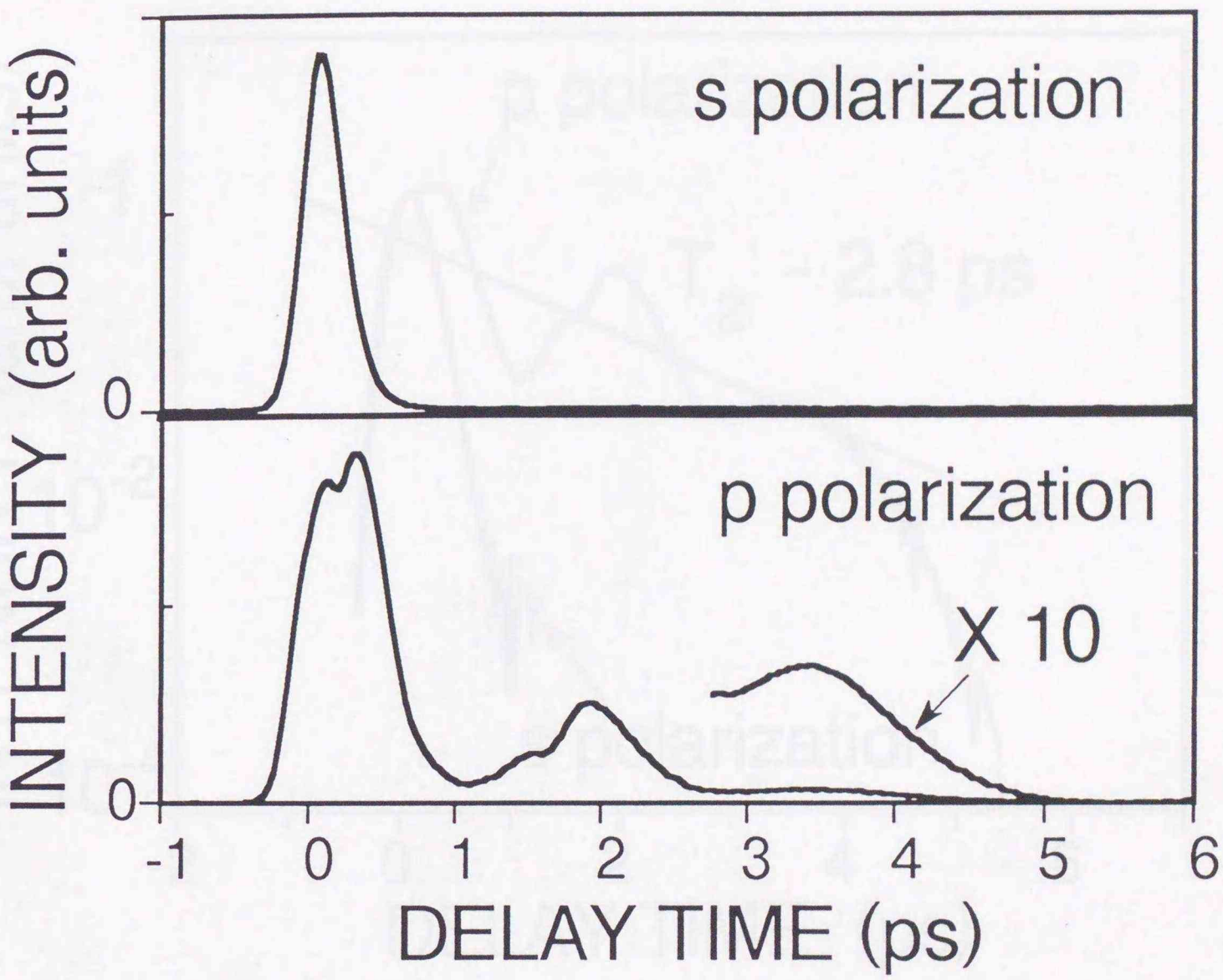

FIG. 2-6. Temporal profile of reflected pulses at Brewster-angle of incidence for the 50-A ZnSe/50-A ZnSSe MQW.

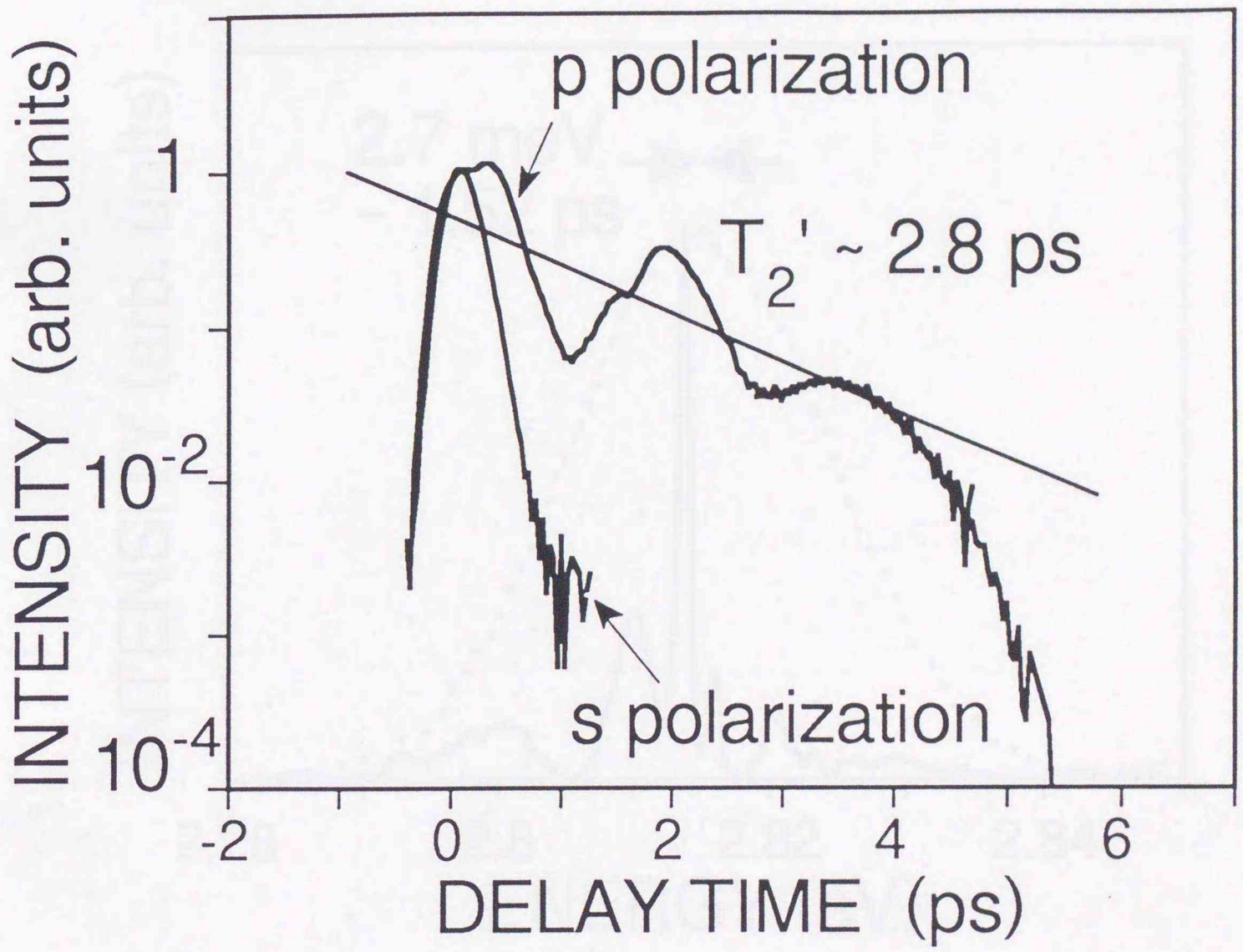

FIG. 2-7. Log plot of TRBR signal for the 50 A/50 A MQW.

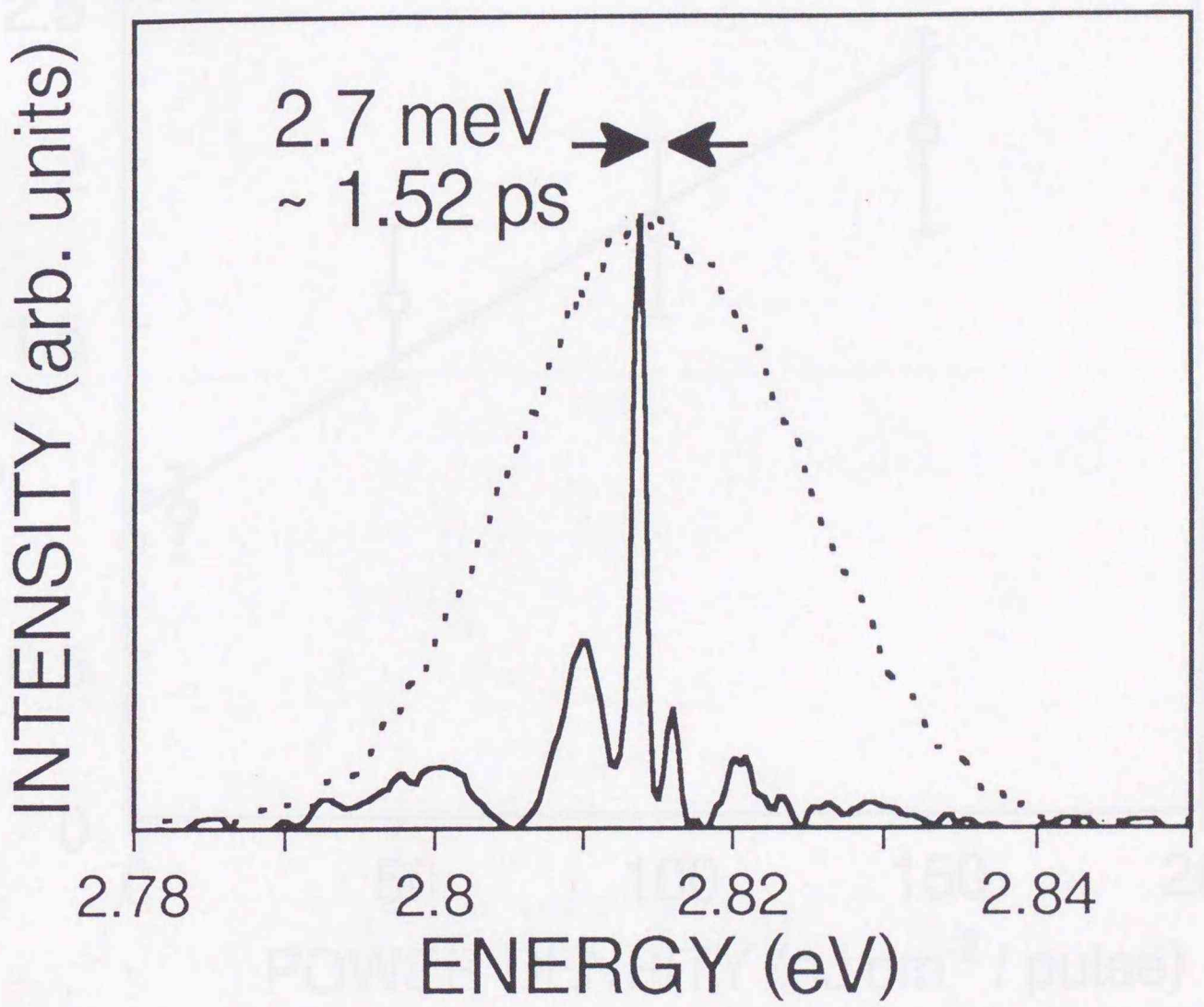

FIG. 2-8. Spectra of an excitation pulse (dotted line) and TRBR pulse (real line) for the 50 A/50 A MQW.

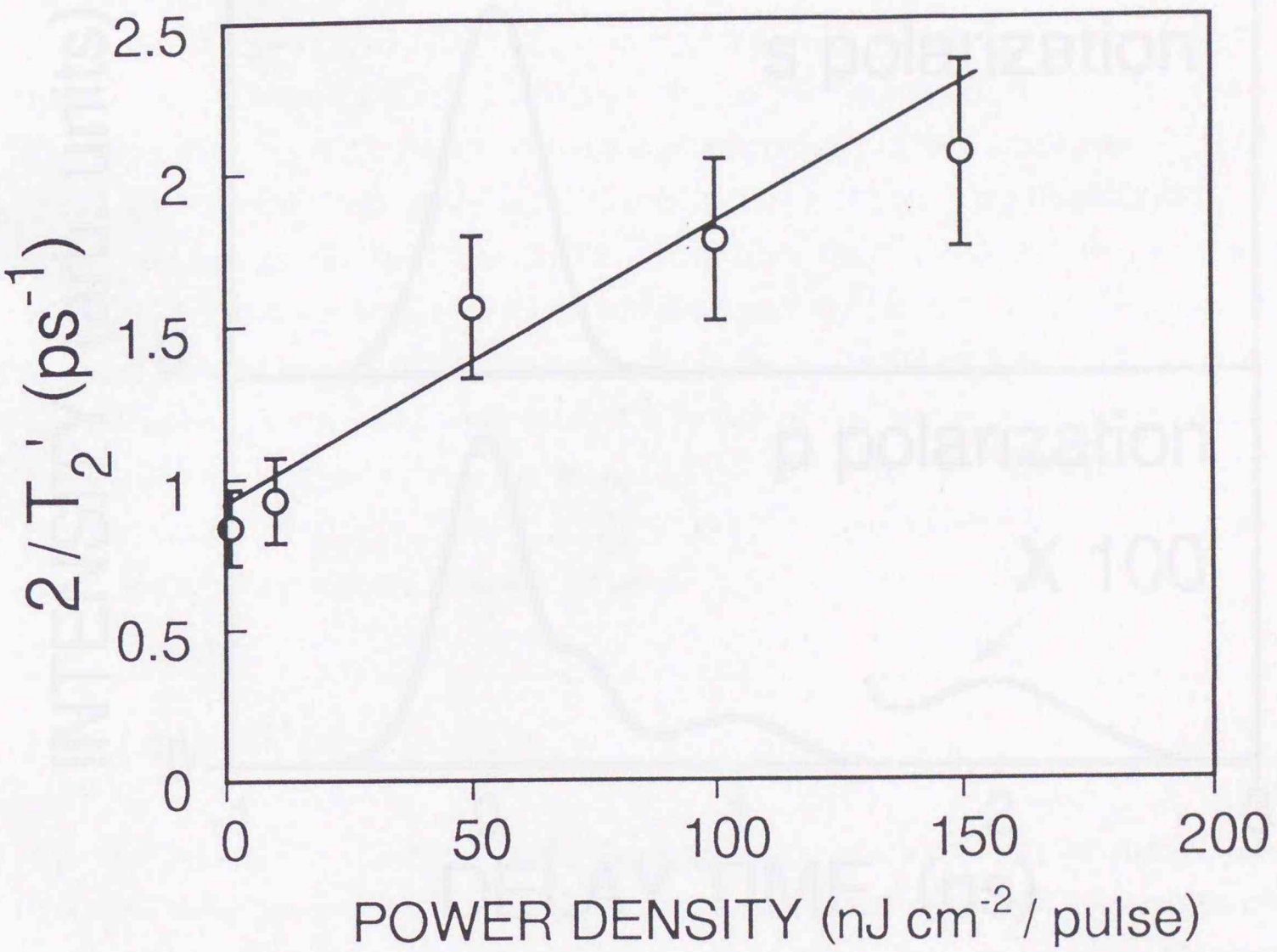

FIG. 2-9. Dependence of the excitation density on the phase relaxation rate for the 50 A/50 A MQW.

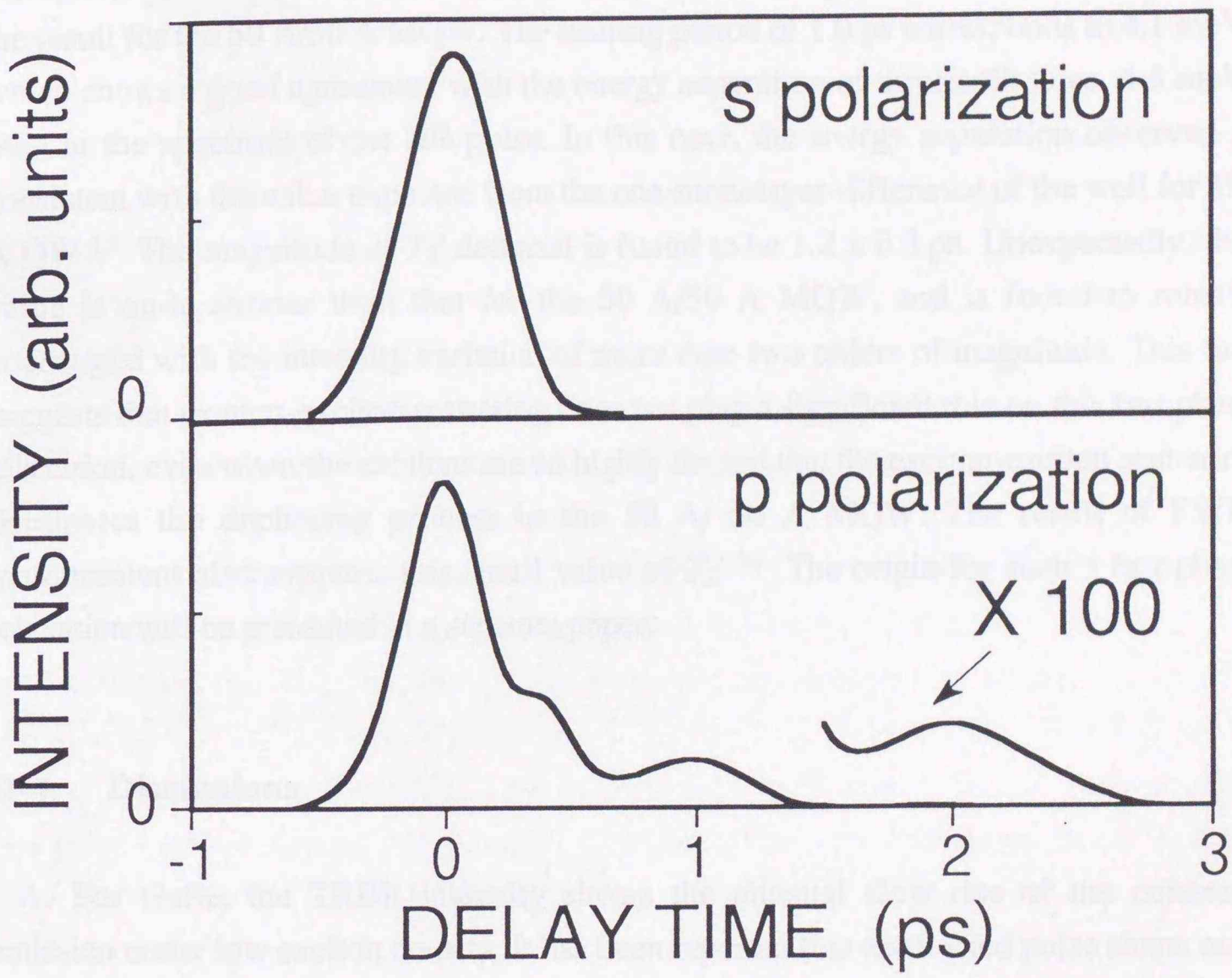

FIG. 2-10. TRBR profile for the 19-A ZnSe/19-A ZnSSe MQW.

shows a linear dependence on the incident intensity. This behavior is a typical dephasing feature due predominantly to incoherent exciton-exciton scattering process. Accordingly, this results indecate that the present procedure gives a correct value of T_2'.

In Fig. 2-10, an example of the TRBR profile for the 19 A/19 A MQW is shown. Except for the faster decaying, the temporal profile is found to be qualitatively similar to the result for the 50 A/50 A MQW. The beating period of 1.0 ps corresponds to 4.1 meV, which shows a good agreement with the energy separation of three split lines, 4-5 meV, seen in the spectrum of the BR pulse. In this case, the energy separation observed is consistent with the value expected from the one-monolayer-difference of the well for 19-A QW.[12] The magnitude of T_2' deduced is found to be 1.2 ± 0.3 ps. Unexpectedly, this value is quite shorter than that for the 50 A/50 A MQW, and is found to remain unchanged with the intensity variation of more than two orders of magnitude. This fact suggests that exciton-exciton scattering does not play a significant role on this fast phase relaxation, even when the excitons are so highly densed that the exciton-exciton scattering dominates the dephasing process in the 50 A/ 50 A MQW. The result of FWM measurement also supports this small value of T_2'.[14] The origin for such a fast phase relaxation will be presented in a separate paper.

II-4. Discussions

For GaSe, the TRBR intensity shows the unusual slow rise of the coherent emission under low exciton density. It has been reported that a reflected pulse shape may be distorted by the effects caused by Brewster-angle of incidence geometry.[15] However, this effect can be observed only under more strict conditions (beam divergence of the incident light is $< 10^{-2}$ degrees) than that of the present experiment. Since the specific time of this temporal feature is a few psec, which is much larger than the pulse duration, but of the same order with T_2, this phenomenon should be a consequence of an intrinsic behavior of coherent excitonic polarization. One probable reason is that a coherent excitonic many-body effect manifests itself in the coherent emission process: Recently it has been pointed out that the generally-accepted noninteracting two-level model is inadequate for describing the transient optical process of excitons, and the coherent emission process is governed by collective effects.[16-21] One typical example of such effects is considered to be so called a local-field effect, where the exciton interacts with not only an applied field but also a self-induced field. The modification on the coherent emission due to local field effects can be obtained by considering a contribution from the

third-order nonlinear polarization in the perturbation treatment of semiconductor Bloch equation. For short pulse excitation, one obtains

$$P(\mathrm{t}) = P(t)^{(1)}{}_{TLS} + P(t)^{(3)}{}_{TLS} + P(t)^{(3)}{}_{SIF} ,$$

where

$$P(t)^{(1)}{}_{TLS} = \mathrm{i}\,\mu\theta \exp[-(T_2^{-1} + \mathrm{i}\Omega)t] \ , \qquad (6,\mathrm{a})$$

$$P(t)^{(3)}{}_{TLS} = -4\,\mathrm{i}\,\mu\theta^3 \exp[-(T_2^{-1} + \mathrm{i}\Omega)t] \ , \qquad (6,\mathrm{b})$$

and

$$P(t)^{(3)}{}_{SIF} = 4\,\mu\theta^3 V t \exp[-(T_2^{-1} + \mathrm{i}\Omega)t] \ . \qquad (6,\mathrm{c})$$

and μ is transition dipole moment, $\theta = \int \mathrm{d}t\ \mu E(t)$ is the pulse area, V represents the relevant exciton binding energy. $P(t)^{(1)}{}_{TLS}$ shows the linear response of FID signals for noninteracting two-level systems, and $P(t)^{(3)}{}_{TLS}$ is the third-order contribution to the above signal. $P(t)^{(3)}{}_{SIF}$ is produced by the self-induced field, which is orthogonal to $P(t)_{TLS}$. The derivation of Eqs. 6.a-b is shown in Appendix. B-2. Eq. 6 shows that nonlinear contribution to the coherent emission is strongly enhanced by local-field effects, that can be estimated as $|P(t)^{(3)}{}_{SIF} / P(t)^{(3)}{}_{TLS}| \sim VT2 = 10 \sim 100$. Such a magnitude can cause a local-field-effects-induced nonlinear signal to appear, and dominate transient response even at very low excitation intensity, so long as short pulse excitation is concerned. The emission intensity, calculated from Eq. 6 with reasonable parameters, is graphically shown in Fig. 2-11. It is found that local-field effects provide a strong enhancement of the coherent signal and give rise to the temporally slow evolution, which is consistent with the experimentally observed behavior intuitively.

It is remarked that although the specific temporal feature may be caused by nonlinear effects, such a feature has not been observed in high intensities. The reason may be that the application to such a high density, of the above mentioned treatment is questionable, since, for example, highly densed free electron-hole pairs may screen Coulomb interaction. The screening effects of Coulomb interaction are likely to reduce or eventually eliminate the specific effects.[22] This explanation seems to account for the experimental results. Furthermore, fast phase relaxation at high densities may diminish the phenomena. Consequently, it is considered that the present interesting behavior can be seen only in an extremely low density condition.

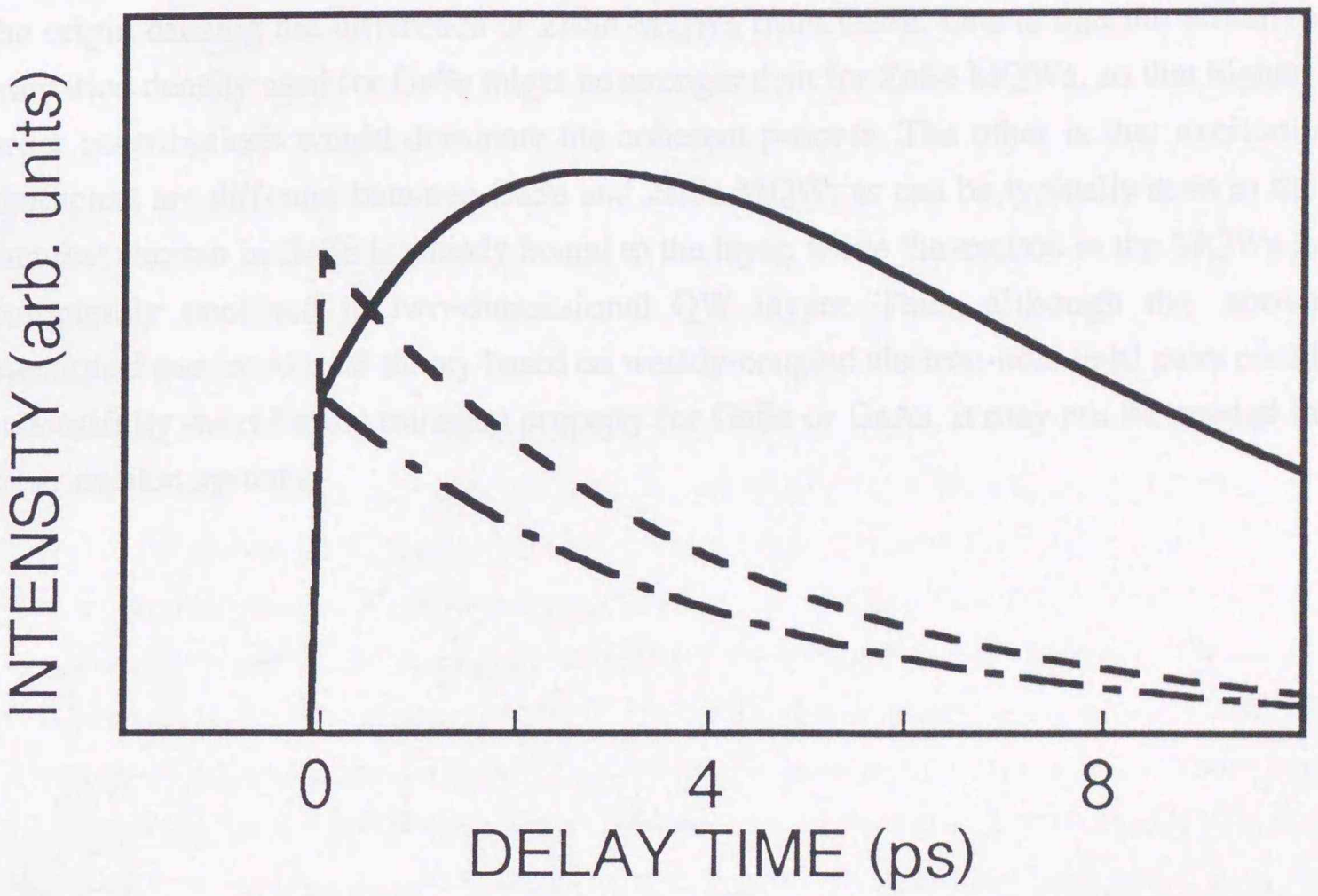

FIG. 2-11. Calculated temporal profile of coherent emission signals, excited by a $\delta(t)$ pulse; the dashed line gives the first-order polarization in Eq. 6.a, and the dash-dotted line includes the contribution of the third-order term, but ignores the local field correction. Used parameters are, $\theta = 0.2$, $T_2 = 8$ ps, and $V = 4.8 \times 10^{12}$ Hz, corresponding to the exciton binding energy of GaSe, 20 meV.

Although the FID signals for GaSe show the characteristic dependence on the excitation density, the signals for ZnSe/ZnSSe MQWs are found to remain unchanged even with changing the intensity by more than three orders of magnitude, except the variation of T_2'. This means that the excitonic transient process in the present ZnSe MQWs is well described by a simple two-level scheme. There may be two possibilities of the origin causing the difference of ZnSe MQWs from GaSe. One is that the effective excitation density used for GaSe might be stronger than for ZnSe MQWs, so that higher-order contributions would dominate the coherent process. The other is that excitonic characters are different between GaSe and ZnSe MQW, as can be typically seen in the fact that exciton in GaSe is weakly bound to the layer, while the exciton in the MQWs is completely confined in two-dimensional QW layers. Thus, although the above mentioned semiconductor theory based on weakly-coupled electron-hole (e-h) pairs could successfully describe the transient property for GaSe or GaAs, it may not be needed in other exciton systems.

III. Coherent emission process studied by time-resolved four-wave-mixing spectroscopy in GaSe [24]

To investigate the phase relaxation process in semiconductors, transient four-wave-mixing (FWM) spectroscopy is known to provide a very powerful tool. FWM signal arises from a third-order nonlinear polarization induced by two successive pulses with time delay. Reflecting the loss of coherence, the intensity of FWM decays with increasing the time between the applied pulses. In case of an inhomogeneously broadened system, the coherent polarization decays due to the interference effect among different resonant frequencies of the exciton states in question. However, the macroscopic polarization can be recovered through FWM process, leading to the emission of photon echo.

Photon echo phenomenon arises when the inhomogeneous broadening dominates the spectrum. In semiconductors, the occurrence of photon echo has been reported for bound-exciton-related transitions in which the homogeneous linewidth is relatively narrow. In many cases of exciton-related transitions, the dephasing time falls in a few picosecond range,[25] that is, the exciton line is broadened due to both homogeneous broadening and inhomogeneous one with the same order of magnitude with each other. It is expected that, in such an intermediate system, the photon echo-type transient response should arise but not be an ordinary one. However, since the short time is involved in the optical process, only the time-integrated intensity of FWM signal has been traced in most studies, where one often fails to grasp correctly the intrinsic behavior of photon echo.

In order to investigate directly this transient process with such a fast phase relaxation involved, we have observed the time-resolved intensity of FWM signals (TRFWM) due to coherent excitons in GaSe. The experiments were carried out by means of adopting the cross-correlation technique to resolve FWM signals temporally in the subpicosecond time region. The TRFWM signals should reflect the coherent emission process caused by a third-nonlinear response.

III-1. Experimental procedure

The sample used in this experiment was a platlet (~4 μm) of ε-GaSe, cleaved with the planes perpendicular to the c axis. These were cooled to 5 K during the measurements. The exciton peaks at ~ 2.11 eV (589 nm) with a width of ~ 8 meV. It is known that excitons in GaSe are confined within a few layers due to stacking disorder, and thereby, these excitons exhibit quasi-two-dimensional characteristics.[26]

The excitation source was a passively mode-locked dye laser which generated pulses with the duration of 0.4 ps. The wavelength of pulses was chosen to cover the exciton resonance energies in the absorption spectrum. Experimental setup is shown in Fig. 3-1. Two beams with wave vectors $\boldsymbol{k}_1$ and $\boldsymbol{k}_2$ were incident on the sample to generate FWM in the so called two-pulse self-diffracted geometry. The excitation intensity was around 10 μJ / cm^2. The FWM signal in the direction $-\boldsymbol{k}_1 + 2\boldsymbol{k}_2$ was mixed with a reference pulse in a BBO crystal and the intensity of the resulting second-harmonic (SH) light was measured as a function of the mutual delay time. It is noted that the SH intensity actually provides the correlation profile between the excitation light and the diffracted light. However, since the excitation light is a coherent transform-limited pulse and the temporal width is sufficiently short compared to the signal, the present data reflect directly the intensity profile of FWM signal.

III-2. Results and discussions

Figure 3-2 shows a series of the temporal development of FWM signals for the different mutual delays between two excitation pulses. In each figure, t_{12} and two arrows represent the time separation and the comes-in times of two pulses, respectively. As t_{12} increases, the time-integrated intensity is seen to decrease, which reflects the homogeneous phase relaxation. It is also observed that FWM signals are pulses and become maximum when a time equal to t_{12} has passed after the second pulse. These behaviors reveal nothing but a transient response of the photon-echo-type, indicating the recovery of the macroscopic polarization. However, in contrast to the conventional photon echoes which have been observed so far,[25, 27] the temporal shape is found to be asymmetric and furthermore, to significantly change with varying t_{12}.

It should be noted that these temporal behaviors are not caused by propagation effects such as the deformation of the diffracted pulse or the change of the coherence property of the light with propagating through a medium. To check this, we compare the temporal form of transmitted pulse and the autocorrelation trace of the excitation pulse. The fact that two forms are almost similar implies that the temporal profile of a resonant light pulse is unchanged with the propagation through the sample.

For simplicity, a two-level model is used to analyze our data. The expression may be derived from the third-order expansion of density matrix formalism. For a two-level system, the third-order nonlinear polarization responsible for scattering into $-\boldsymbol{k}_1+2\boldsymbol{k}_2$ is expressed as

$$P(\boldsymbol{r}, t) \sim \begin{cases} \exp[(-\boldsymbol{k}_1 + 2\boldsymbol{k}_2) \bullet \boldsymbol{r}] \exp[-(t - t_1)\, T_2^{-1}]\, G(t - t_2 - t_{12}) , & t > t_2 \\ 0 , & t < t_2 \end{cases}$$

and

$$G(\tau) = \int_0^\infty \mathrm{d}(\Delta\omega)\, g(\Delta\omega) \exp(\mathrm{i}\, \Delta\omega\tau) \quad , \tag{1}$$

where t_i is the arrival time of the i-th pulse, T_2 is the homogeneous phase relaxation time, $\Delta\omega$ is the frequency detuning defined as the difference between the material resonance frequency and the laser one, and $g(\Delta\omega)$ is the distribution function characterizing the inhomogeneous broadening. The derivation of these equations are presented in Appendix B. T_2* is used to refer to the characteristic width of $G(\tau)$. The signal intensity is found to be the multiplication of the single exponential curve which decays from $t = t_1$, with $G(\tau)$ which is centered at $t = t_2 + t_{12}$. The former represents the homogeneous decay due to the dynamical relaxation and the latter, the recovery of macroscopic polarization due to FWM process.

When $T_2 >> T_2$* in which conventional photon echoes may be observed, the temporal shape of FWM signal only reflects $G(\tau)$, which is of a symmetric pulse form and is unchanged for different t_{12}. If $T_2 \sim T_2$* which corresponds to the present case, the signal should reflect not only the above mentioned symmetric property but also the fast decay of the homogeneous phase relaxation. This is the reason that the observed signal is asymmetric. Moreover, in such a case the temporal shape can change for different t_{12} since the signal is observed only for $t > t_2$.

It should be emphasized that, if only the time-integrated intensity is traced, the homogeneous dephasing time could be obtained only when the resonance line is either completely homogeneously or inhomogeneously broadened. Furthermore, in the intermediate system, it is not simple to estimate T_2 correctly from the time-integrated signal. On the other hand, with paying attention to the time-dependent intensity at $t = t_2 + t_{12}$ for different t_{12}, the homogeneous dephasing time can be obtained exactly in principle, since the intensity at $t = t_{12}$ is completely independent of $G(\tau)$, which is easily seen in Eq. 1. Applying this treatment to the present data, the homogeneous dephasing time is found to be 3.8 ps. Moreover, the calculated profiles of $G(\tau)$ for different t_{12}, which are given by Eq. 1 with T_2 = 3.8 ps, are almost similar to each other. This indicates that our interpretation may be correct. With using the above mentioned T_2 and the typical profile of $G(\tau)$, the curve of the time-dependent intensity can be obtained. As can be seen in Fig. 3-3, the calculated curves are in fairly good agreement with experimental data.

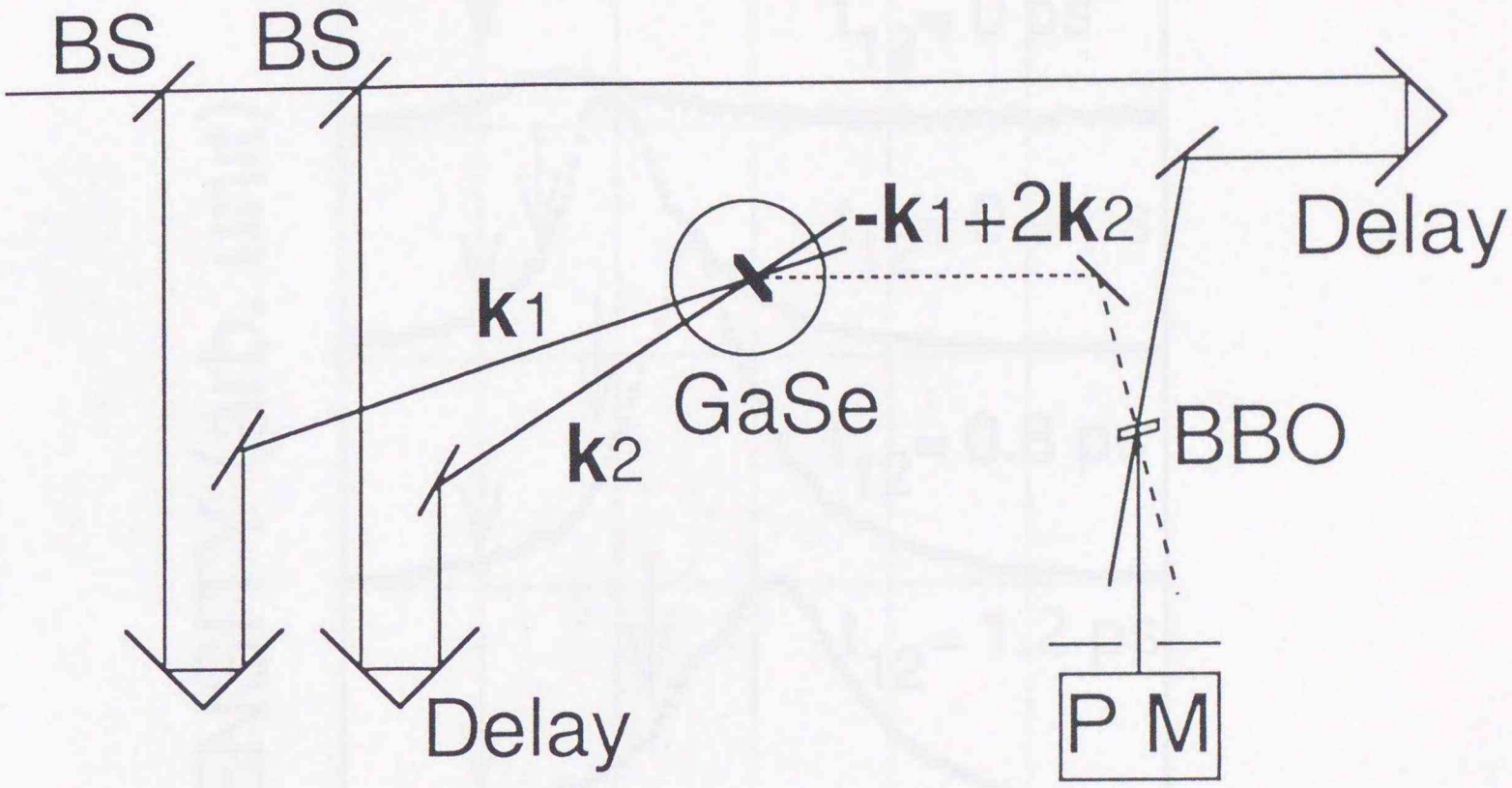

FIG. 3-1. Experimental setup of time-resolved four-wave-mixing spectroscopy.

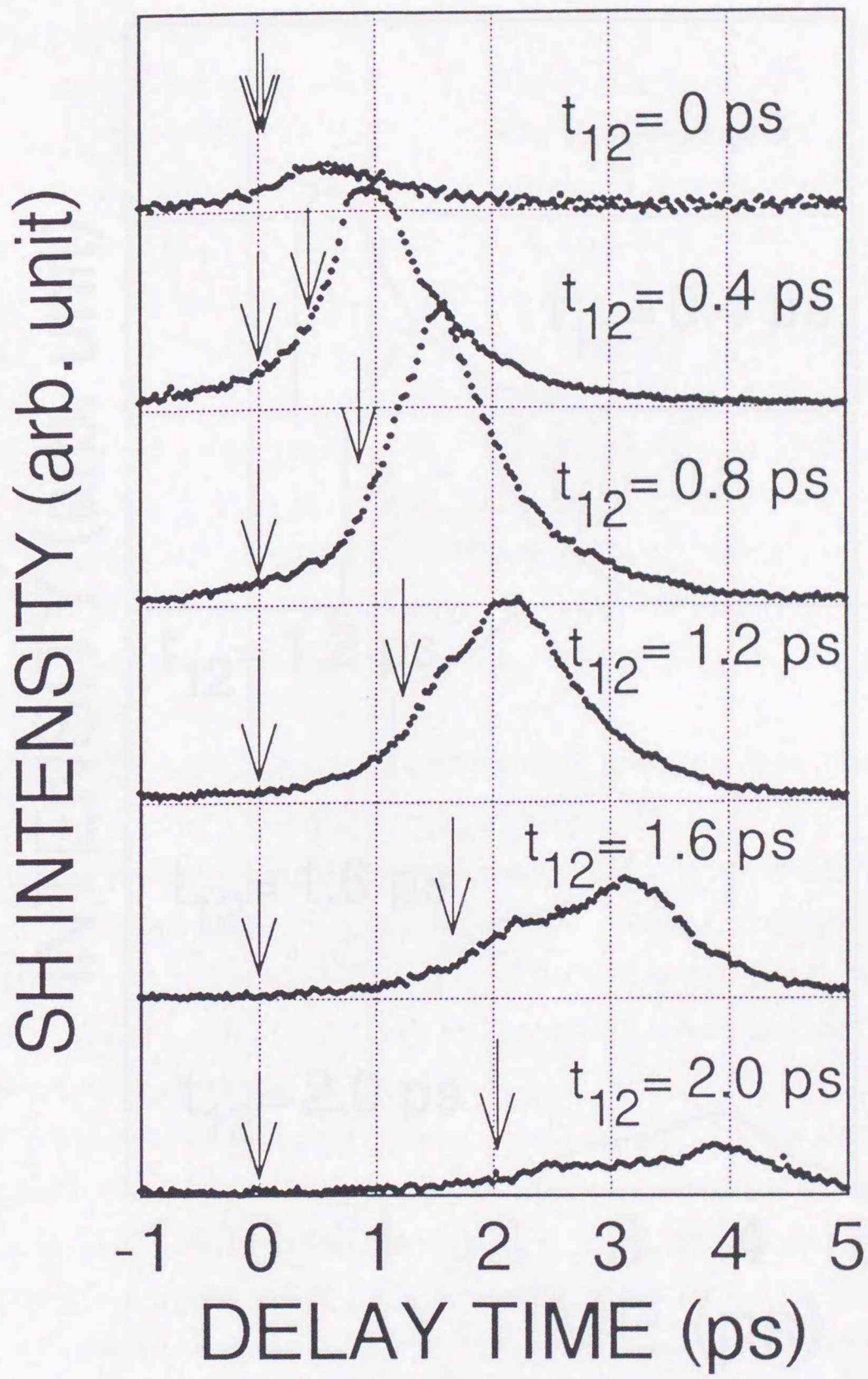

FIG. 3-2. Time-resoved four-wave-mixing signals for GaSe.

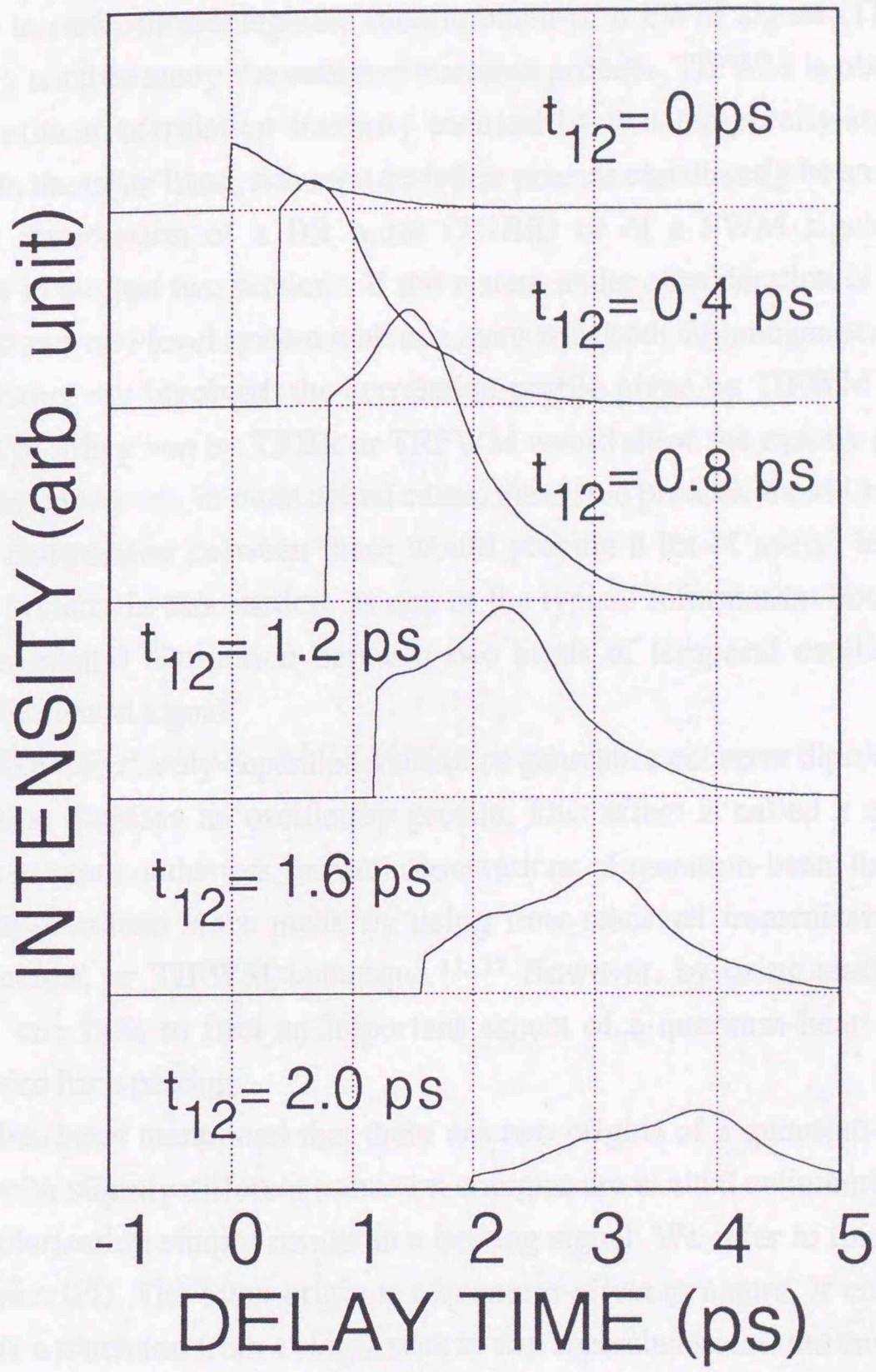

FIG. 3-3. Calculated cuurves of four-wave-mixing signals.

IV. Experimental distinction between classical- and quantum interference effect

Up to now, time-integrated measurement of a FWM signal (TIFWM) has been frequently used to study the coherent transient process. TIFWM is observed as a third-order nonlinear correlation intensity induced by two temporally-separated resonant pulses. On the other hand, coherent emission process can directly be studied by the time-resolved observation of a BR pulse (TRBR) or of a FWM signal (TRFWM), as discussed in the last two sections. If the system under consideration is simple enough to be treated as a two-level system with one atom with both inhomogeneous broadening and level splitting not involved, the correlation profile given by TIFWM and the coherent emission profile given by TRBR or TRFWM would show the exactly same feature with each other. However, in most actual cases, these two profiles should be different. Thus, detailed comparison between them would provide a lot of useful information of the relevant system. In this section, as one of the typical information obtained, we discuss the experimental distinction between two kinds of temporal oscillation seen in the coherent emission signal.

When two closely-separated transitions generate a coherent dipole, the macroscopic polarization displays an oscillatory profile. This effect is called a quantum-beat. For excitons in semiconductors, several observations of quantum-beats have been reported. These observations were made by using time-resolved transmission,[9] reflection,[6-8] luminescence, or TIFWM technique.[11, 17] However, by using such an experimental method, one fails to find an important aspect of a quantum-beat; the origin of the interference for a beating.

It has been mentioned that there are two origins of a quantum-beat: First, if two dipoles with slightly different transition energies are excited coherently, the interference of the polarization simply results in a beating signal. We refer to this as a *polarization interference*(PI). The other origin is a quantum-effect in nature. If coherent emission is caused by a transition from a single state to two separated states, the emitted light displays also a beating signal. We refer to this as a *quantum-beat* (QB), since it should arise from the interference of two wave functions. Although the definition of QB and PI is simple, it becomes difficult to distinguish these two beats experimentally, since the spectra for both cases are composed of similar split lines, and the coherent emission signal exhibits a similar oscillatory profile. However, the signal emitting from the nonlinear origin should provide different features between PI and QB. Thus, by comparing TIFWM and

TRFWM (or TRBR), one can understand which origin induces the beat, thereby enabling one to clarify physical origin of the relevant energy separation.

After a brief theoretical consideration of PI and QB, we discuss the case for GaSe in IV-2, where the comparison between TIFWM and TRFWM reveals that the temporal oscillation observed arises from QB between singlet and triplet exciton states involved. In IV-3, we compare TRBR and TIFWM signal profiles for the ZnSe/ZnSSe MQW's, where both QB and PI are found to appear on the coherent emission signal.

IV-1. Theoretical consideration for polarization interference and quantum beat found in four-wave-mixing signal

We briefly examine the temporal profile of FWM signals. First we consider the situation for realizing PI. In this case, the signal is simply expressed as the superposition of two independent polarizations with the different energies of Ω_1 and Ω_2. For simplicity, we assume that the incident pulses are described in terms of a δ-function, and the inhomogeneous broadening is neglected. By the perturbation treatment of the density matrix formulation, the temporal development of the induced polarization for PI is given by

$$P_{\mathrm{PI}}(\tau,t) = \mu A\, g(\tau,t) \quad , \qquad [1.a]$$

$$A = -2\,i\,N\,\theta_1\theta_2^2 \quad , \qquad [1.b]$$

$$g(\tau,t) = e^{-\gamma t}\left[w_1 e^{-i\Omega_1 (t-2\tau)} + w_2 e^{-i\Omega_2 (t-2\tau)}\right]\Theta(t-\tau) \quad , \qquad [1.c]$$

where τ is a time separation between two excitation pulses, μ is the transition matrix element, γ is the transverse relaxation rate, N is the density of the dipole, $\theta_j = \int_{-\infty}^{\infty} dt\ \mu E_j(t)$ denotes the pulse area of the j-th pulse, $w_{1,2}$ shows the spectral weight for the two lines, and Θ is the step function.

On the other hand, QB arises from the transition from two split levels to a single state. Thus it is necessary to consider the coherent transient response for a three-level system. As a result, the FWM signal for QB can be derived as

$$P_{QB}(\tau,t) = \mu_1 A\, F(\tau) f(t-\tau) \quad , \qquad [2.a]$$

$$F(\tau) = e^{(i\Omega_1 - \gamma_1)\tau} + c^2 e^{(i\Omega_2 - \gamma_2)\tau} \quad , \qquad [2.b]$$

$$f(t-\tau) = \left[e^{(-i\Omega_1 - \gamma_1)(t-\tau)} + c^2 e^{(-i\Omega_2 - \gamma_2)(t-\tau)} \right] \Theta(t-\tau) \quad , \qquad [2.c]$$

where $\mu_{1\,(2)}$, $\gamma_{1\,(2)}$ and $\Omega_{1\,(2)}$ are the relevant magnitudes labeled the transition no. 1 (2), and $c = \mu_1/\mu_2$. The derivation of above equations is presented in Appendix C.

The temporal development of FWM signal intensity is graphically shown in Fig. 4-1. The typical difference between for QB and PI is : (i) For the given time delay τ, TRFWM (or TRBR) similarly displays a beating with the frequency of $\Omega_2 - \Omega_1$. However, the phase of the oscillation is different, that is, the amplitude becomes maximum at $t = \tau$ for QB, and at $t = 2\tau$ for PI, respectively. (ii) By changing τ, the entire profile for QB also changes, while it is unchanged for PI. Then the modulation depth seen in the TIFWM for PI should be smaller (or even diminished) than that of QB. As seen in Fig. 4-1, one can clearly discriminate whether the beat seen in the coherent emission arises from a quantum or classical interference effect.

IV-2. Four-wave-mixing quantum beat in GaSe [28]

In Fig. 4-2, TIFWM signal for GaSe is shown. This figure was observed at oblique incidence with the incident angle of around 30°. It was found that, for p polarization, an oscillatory structure was superimposed on the decay profile, but this oscillation disappeared for s polarization. Furthermore, it was confirmed that the beating structure was not found at nearly normal incidence. Such a polarization dependence implies that this beat is caused by the splitting of singlet and triplet excitons: The exciton in GaSe splits into higher singlet and lower triplet states due to the exchange interaction. [29] The singlet exciton is optically active for the polarization $E /\!/ c$, while the triplet exciton is allowed for $E \perp c$. Consequently, both exciton states can be excited simultaneously by obliquely incident p-polarized light. It is remarked that the oscillatory profile presented in Ref. [11] is clearer than the present data. This is probably due to the fact that the excitation pulse has the small wing-like component caused by the pulse compression procedure.

Although the result suggests that the beating arises from the split singlet and triplet exciton states, it is known that the exciton line in GaSe is composed of a few variations of confinement states due to the random stacking faults. [26] Thus it is possible to postulate that the observed beating results from this spatial structure. In order to obtain the direct evidence for the origin of this structure, we resolved the FWM signals temporally.

In Fig. 4-3, a series of TRFWM signals is displayed. In each curve, the first pulse was incident on the sample at $t = 0$ and the arrival time of the second pulse was changed. It is found that the entire feature of the emitted signal changes with varying the pulse separation, resulting in a beating seen in the time-integrated intensity. Such a temporal profile is an expected feature for QB.

In Fig. 4-4, temporal shapes of FWM signals for several time delays are shown. The emitted signal also displays an oscillatory structure. The time periodicity is almost the same with that in the time-integrated measurement. Furthermore, considering the finite pulse duration, it is seen that the signal amplitude becomes maximum at the incidence of the second pulse, reflecting the phase of this oscillation. This is just an expected behavior for QB. As a result, it is concluded that the present beating arises from the quantum-interference effect, and the corresponding spectral splitting originates from the separation between the singlet and triplet excitons.

Although the temporal feature can be shown to be qualitatively reproduced in terms of Eq. 2, there are some differences between the expected curves and the experimental data. One of the reasons may come from the fact that we neglect the influence of the inhomogeneous broadening. By considering this, the signals would show a pulse-like shape which is located at $t = 2\tau$. The experimental result displays the increase of FWM signals around $t = 2\tau$. It suggests that the present system belongs to the intermediate regime of homogeneously and inhomogeneously broadened transitions, as already mentioned in Section III.

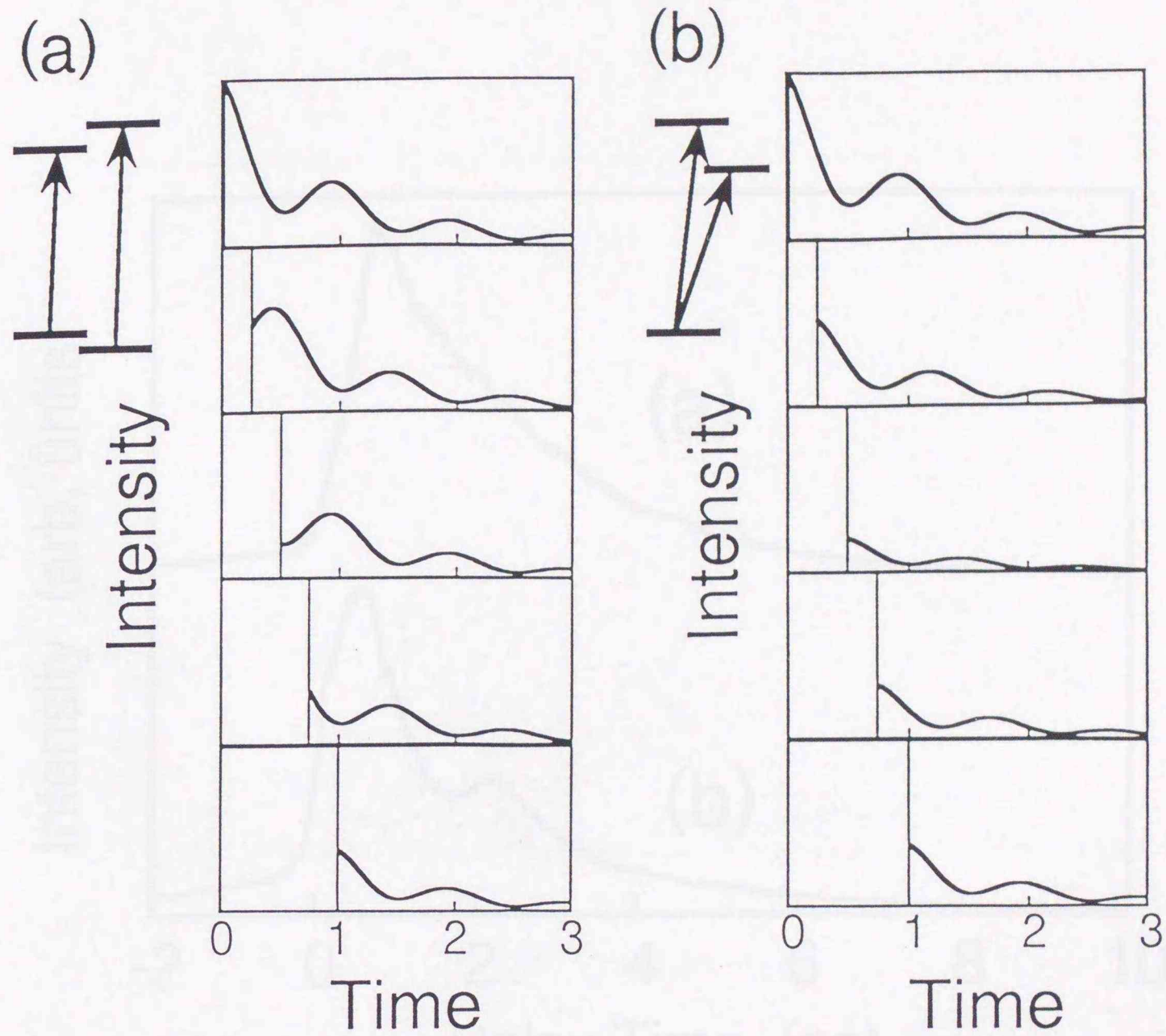

FIG. 4-1. Calculated temporal profile of FWM signals for (a) the case of PI, from Eq. 1 with $\Omega_1 - \Omega_2 = 1$, $\gamma = 0.5$, and $w_2/w_1 = 2 - \sqrt{3}$, and (b) the case of QB, from Eq. 2 with $\Omega_1 - \Omega_2 = 1$, $\gamma_1 = \gamma_2 = 0.5$, and $c^2 = 2 - \sqrt{3}$. The parameters for (a) and (b) give the same absorption spectra.

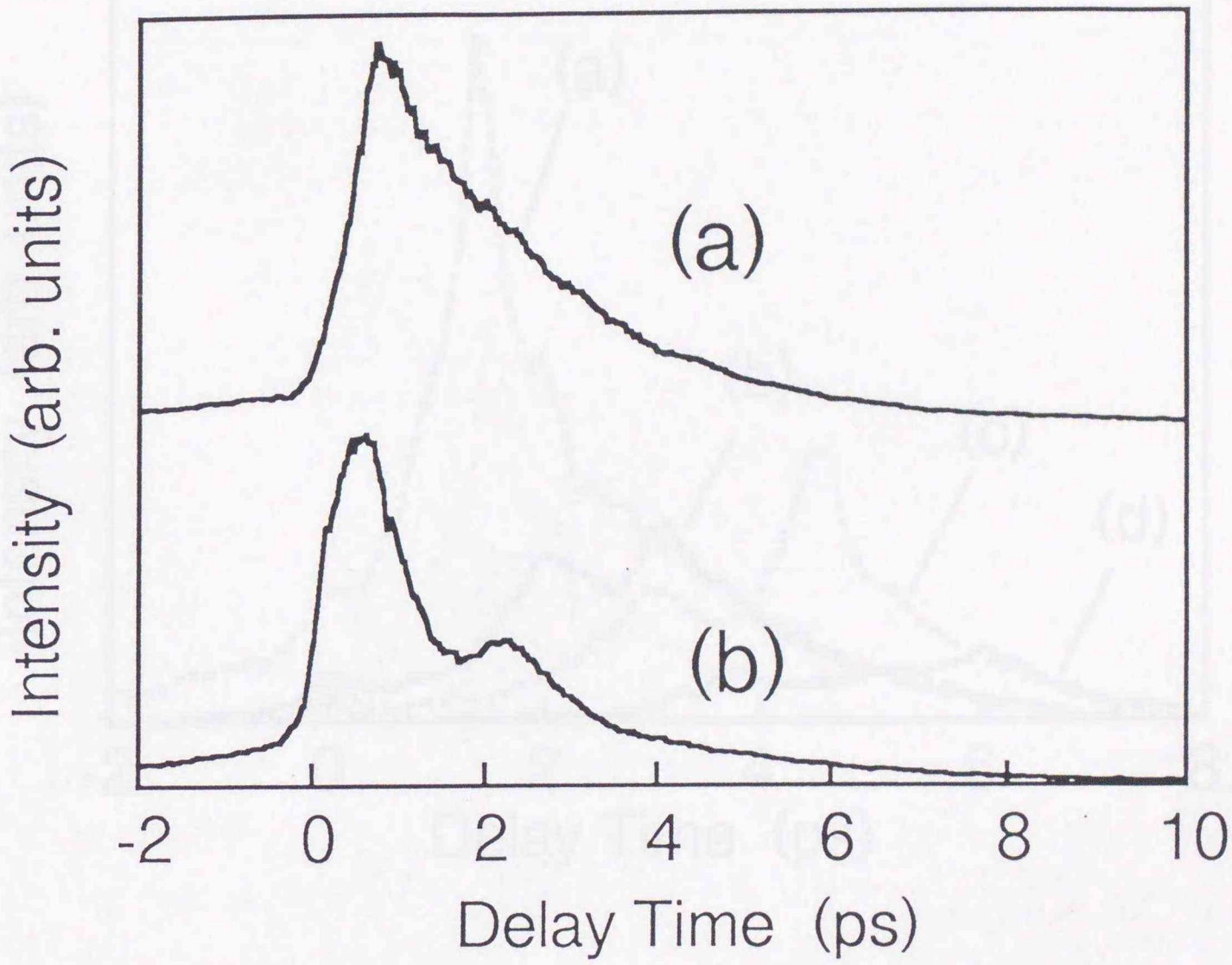

FIG. 4-2. Time-integrated FWM signals for GaSe at oblique incidence with (a) s polarization, and (b) p polarization.

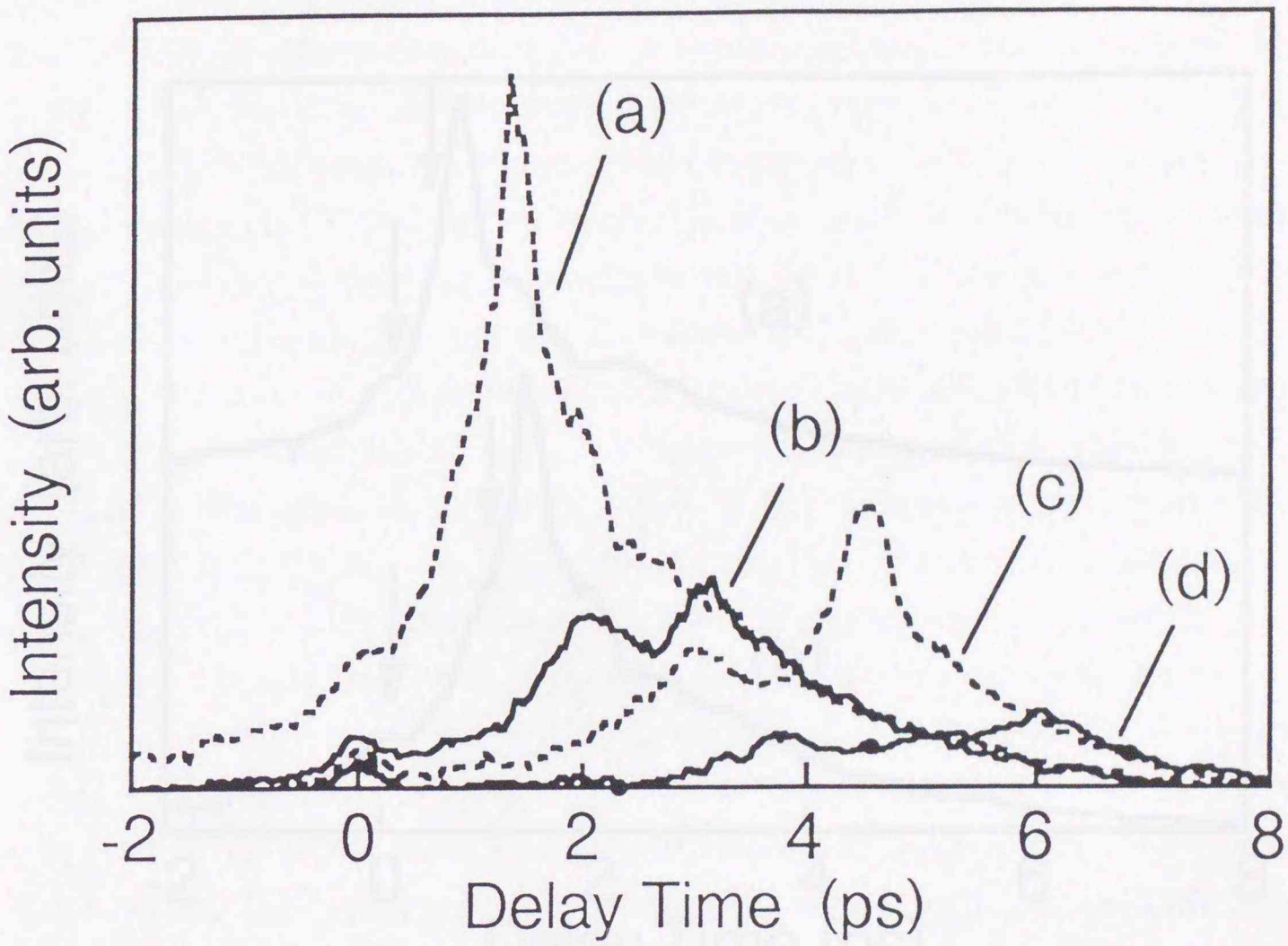

FIG. 4-3. Temporally-resolved FWM signals for (a) $\tau = 0.8$ ps, (b) 1.6 ps, (c) 2.4 ps, and (d) 3.2 ps.

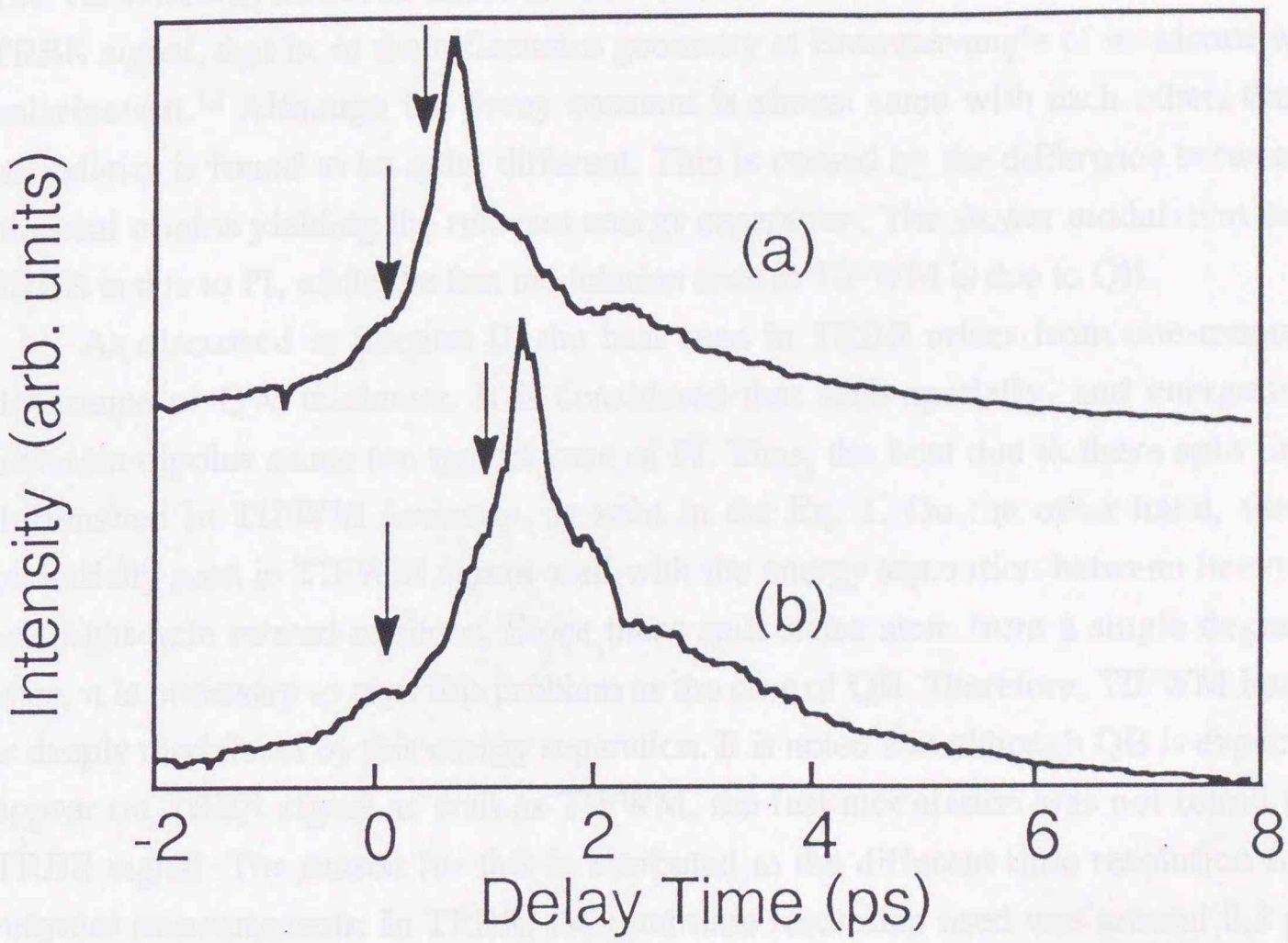

FIG. 4-4. Temporally-resolved FWM signals for (a) $\tau = 0.4$ ps, and (b) 0.8 ps. Arrows indicate the center incident times of the finite pulses.

IV-3. Coexistence of polarization interference and quantum beat: the case of ZnSe/ZnSSe multiple quantum wells [30]

In Fig. 4-5, the TIFWM signal observed for the 50-A ZnSe/50-A ZnSSe MQW is shown, together with the coherent emission signal observed by TRBR for comparison. The TIFWM was observed under almost the same excitation condition with that for the TRBR signal, that is, in the reflectance geometry at Brewster-angle of incidence with p polarization.[14] Although the decay constant is almost same with each other, the beat periodicity is found to be quite different. This is caused by the difference between the physical origins yielding the relevant energy separation: The slower modulation seen in TRBR is due to PI, while the fast modulation seen in TIFWM is due to QB.

As discussed in Section II, the beat seen in TRBR arises from one-monolayer difference of QW thickness. It is considered that such spatially- and energetically-different dipoles cause the typical case of PI. Thus, the beat due to these split lines is diminished in TIFWM intensity, as seen in the Eq. 1. On the other hand, the beat periodicity seen in TIFWM agrees well with the energy separation between heavy-hole and light-hole related excitons. Since these split states stem from a single degenerate state, it is necessary to treat this problem as the case of QB. Therefore, TIFWM intensity is deeply modulated by this energy separation. It is noted that although QB is expected to appear on TRBR signal as well as TIFWM, the fast modulation was not found in the TRBR signal. The reason for this is attributed to the different time resolution for the relevant measurements. In TRBR, the total time resolution used was around 0.3 ps, so that such a fine modulation could not be detected distinctly.

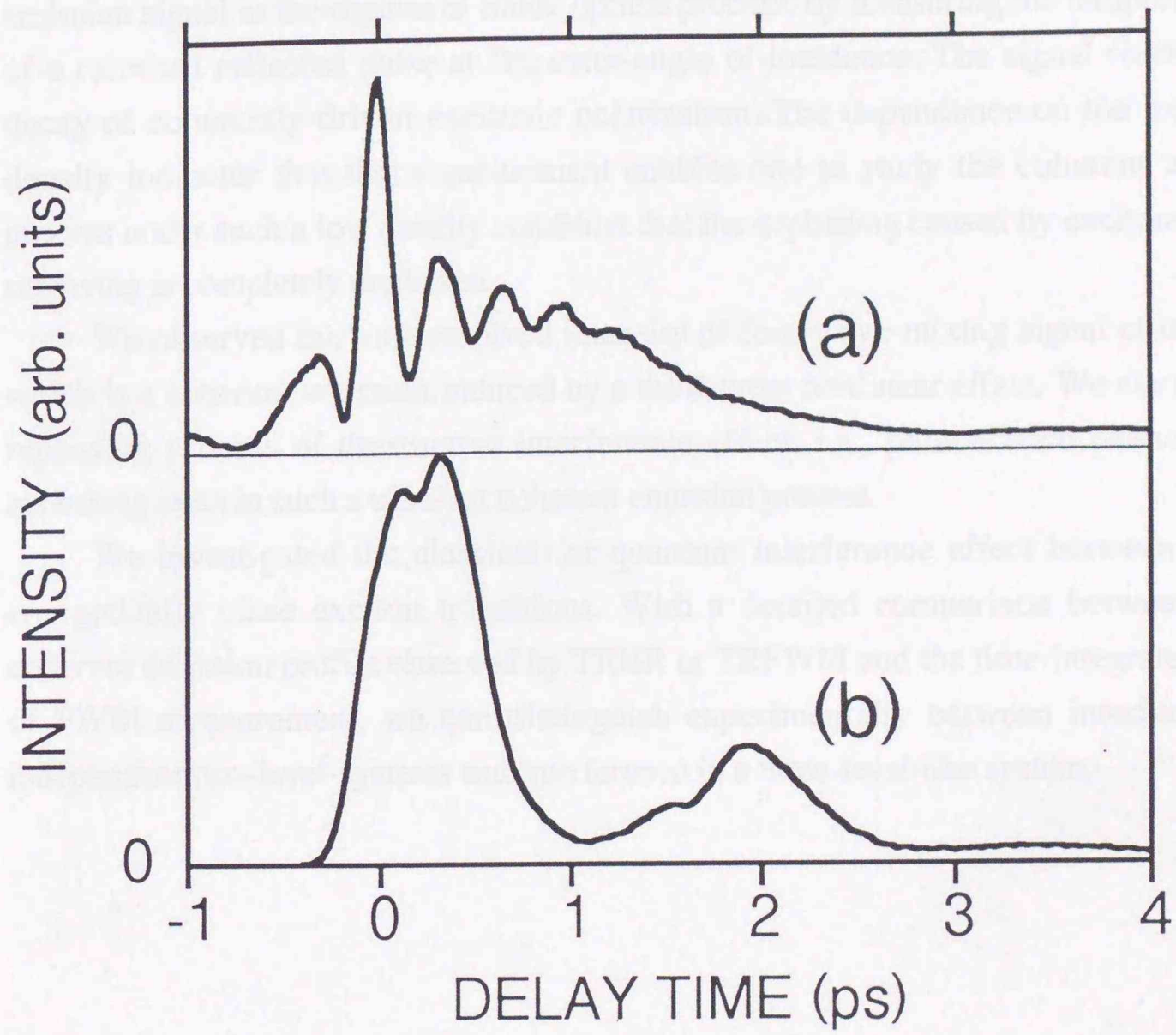

FIG. 4-5. Temporal profile of (a)Time-integrated FWM signal and (b) TRBR profile, for the 50-A ZnSe/50-A ZnSSe MQW.

V. Conclusions

Coherent transient spectroscopy has been frequently used to study the phase relaxation property of electronic transitions in semiconductors. Here, we have reported the first observation of coherent emission process of excitons in subpicosecond domain, by means of two newly-developed methods. We observed a background-free coherent emission signal in the regime of linear optical process, by measuring the temporal shape of a resonant reflected pulse at Brewster-angle of incidence. The signal showed free decay of coherently-driven excitonic polarization. The dependence on the excitation density indicates that this measurement enables one to study the coherent transient process under such a low density condition that the dephasing caused by exciton-exciton scattering is completely neglected.

We observed the time-resolved intensity of four-wave-mixing signal of excitons, which is a coherent emission induced by a third-order nonlinear effect. We clarified the rephasing process of destructive interference effect, i.e., photon echo phenomenon, appearing even in such a ultrafast coherent emission process.

We investigated the classical- or quantum interference effect between several energetically close exciton transitions. With a detailed comparison between direct coherent emission profile observed by TRBR or TRFWM and the time-integrated signal of FWM measurement, we can distinguish experimentally between interference of independent two-level-systems and interference in a three-level-like system.

Acknowledgments

The author wishes to thank Professor Kuon Inoue for many hours of helpful discussions and for suggesting the problem. He also wishes to thank Professor Fujio Minami for illuminating discussions. He wishes to acknowledge Professor Ikuo Suemune for providing the ZnSe/ZnSSe samples and for discussions on the growth mechanism. He thanks to Kouji Yoshida, Masaki Hayashi, and Ryosuke Kuriayashi for their experimental assistance.

References

[1] D. Fröhlich, A. Kuik, B. Uebbing, A. Mysyrowicz, V. Langer, H. Stolz, and W. von. der Osten, *Phys. Rev. Lett.* **67**, 2343 (1991).

[2] T. Kuroda, M. Hayashi, K. Inoue, K. Yoshida, F. Minami, and H. Fujiyasu, *J. Appl. Phys.* **76**, 533 (1994).

[3] K. Inoue, T. Kuroda, F. Minami, K. Yoshida and M. Hayashi, *J. Cryst. Growth* **138**, 182 (1994).

[4] J. Aaviksoo and J. Kuhl, *IEEE J. Quntum Electr.* **QE25**, 2523 (1989).

[5] J. Aaviksoo, J. Kuhl, and I. Reimand, *Solid State Commun.* **72**, 49 (1989).

[6] A. Hasegawa, T. Kuroda, K. Inoue, Y. Mitsumori, F. Minami, and K. Era, *J. Lumin.* **58**, 234 (1994).

[7] T. Kuroda, K. Inoue, I. Suemune, R. Kuribayashi, and F. Minami, *Proceedings of Int'l. Conf. on Excitonic Process in Condensed Matter*, at Darwin, July 1994, in press.

[8] T. Kuroda, K. Inoue, F. Minami, and I. Suemune, *Proceedings of 22nd. Int'l. Conf. on Phys. Semicond.*, at Vancouver, August 1994 (World Scientific), in press.

[9] T. Mishina and Y. Masumoto, *Phys. Rev. Lett.* **71**, 2785 (1993).

[10] F. Minami, A. Hasegawa, T. Kuroda, and K. Inoue, *J. Lumin.* **53**, 371 (1992).

[11] A. Hasegawa, F. Minami, and K. Inoue, *Proc. 21st. Int. Conf. on Phys. Semicond.* (World Scientific, Singapore, 1992), p. 221.

[12] K. Inoue, T. Kuroda, K. Yoshida, and I. Suemune, unpublished.

[13] Y. Kuroda, I. Suemune, Y. Fujii, and M. Fujimoto, *Appl. Phys. Lett.* **61**, 1182 (1992).

[14] T. Kuroda and K. Inoue, unpublished.

[15] I. H. Cambell and P. M. Fauchet, *Optics Lett.* **18**, 634 (1988).

[16] See for example; S. W. Koch, N. Peyghambarian, and A. Mysyrowicz, *Introduction of Semiconductor Optics* (Prentice Hall, New York, 1993).

[17] K. Leo, E. O. Göbel, T. C. Damen, J. Shah, S. Schmitt-Rink, W. Shäfer, J. F. Müller, K. Köhler, and P. Ganser, *Phys. Rev. B* **44**, 5726 (1991).

[18] K. Leo, M. Wegener, J. Shah, D. S. Chemla, E. O. Göbel, T. C. Damen, S. Schmitt-Rink, and W. Shäfer, *Phys. Rev. Lett.* **65**, 1340 (1990).

[19] M. Wegener, D. S. Chemla, S. Schmitt-Rink, and W. Shäfer, *Phys. Rev. A* **42**, 5675 (1990).

[20] S. Weiss, M. -A. Mycek, J. -Y. Bigot, S. Schmitt-Rink, and D. S. Chemla, *Phys. Rev. Lett.* **69**, 2685 (1992).

[21] D. S. Kim, J. Shah, T. C. Damen, W. Shäfer, F. Jahnke, S. Schmitt-Rink, and K. Köhler, *Phys. Rev. Lett.* **69**, 2725 (1992).

[23] Reduction of Coulomb interaction effects due to highly densed free carriers has also been reported in Ref. [21].

[24] T. Kuroda, F. Minami, and K. Inoue, *Proc. 21st. Int. Conf. on Phys. Semicond.* (World Scientific, Singapore, 1992), p. 1799.

[25] G.Noll, U.Siegner, S.G.Shevel, and E.O.Gobel, *Phys.Rev.Lett.* **64**, 792 (1990).

[26] J.J.Forney, K. Maschke, and E. Mooser, *J.Phys.* **C10**, 1887 (1977).

[27] M.D.Webb, S.T.Cundiff, and D.G.Steel, *Phys.Rev. Lett.* **66**, 934 (1991).

[28] T. Kuroda, F. Minami, and K. Inoue, unpublished.

[29] E. Mooser and M. Shulter, *Nuovo Cimento* **B18**, 164 (1973).

[30] T. Kuroda, K. Inoue, R. Kuribayashi, and I. Suemune, unpublished.

[31] T. Yajima and Y. Taira, *J. Phys. Soc. Jpn.* **47**, 1620 (1979).

APPENDICES

Excitonic Coherent Emission Process in Semiconductors

Takashi Kuroda

APPENDICES

Appendix A. General description for coherent emission process in the linear regime

From the macroscopic point of view, any linear optical process, such as transmission, absorption, etc., is determined by the complex dispersion relation, $\omega(k)$. Microscopically, on the other hand, this optical process can be expressed in the superposition of coherently-emitted radiations from each dipole, and the self-consistent treatment of an emitted and applied fields must result in the expression of the dispersion relation.

In this Appendix, we derive theoretically the temporal shape of reflected or transmitted light pulse near a resonant region. Although the material constants are expressed only in terms of the dispersion relation, the time-resolved signal of the output pulse reflects the coherent emission process, showing the decay profile at the trailing tail. Furthermore, when we adopt the reflectance configuration at Brewster-angle of incidence, the coherent-polarization-related signal can be observed clearly, with the nonresonant contribution eliminated.

The temporal shape of output pulses are expressed as

$$E_{out}(t) = \int_{-\infty}^{\infty} d\tau\, G(\tau)\, E_{in}(t-\tau) \qquad (1.a)$$

$$= \int_{0}^{\infty} d\omega\, \tilde{G}(\omega)\, E_{in}(\omega)\, e^{i\omega t} \quad , \qquad (1.b)$$

where E_{in}, and $E_{out}(t)$ are the temporal form of the input and output pulse, respectively, E_{in}, and $E_{out}(\omega)$ are the Fourier transform of them, and $G(\tau)$ represents a response function which is given by Fourier transform of the frequency dispersion of the relevant optical process $G(\omega)$. When the incident pulse is short enough to be approximated by a δ function, $E_{out}(t)$ can be equal to $G(t)$. The intensity of output light is given by,

$$I(t) \propto |E_{out}(t)|^2 \quad . \qquad (2)$$

The dispersion relation is expressed as $k(\omega)$, $n(\omega)$, or $\varepsilon(\omega)$, which are the complex wavevector, refractive index, and dielectric function, respectively. k, n, and ε are related to each other, as

$$k(\omega) = \frac{\omega}{c} n(\omega) \quad , \tag{3}$$

$$n(\omega) = \sqrt{\varepsilon(\omega)} \quad , \tag{4}$$

where c is the light velocity in vacuum. The dielectric function under consideration is described as

$$\varepsilon(\omega) = \varepsilon(\infty) + \frac{4\pi\beta\omega_0^2}{\omega_0^2 - \omega^2 - i\gamma\omega} , \tag{5}$$

where $\varepsilon(\infty)$ is the background dielectric constant, ω_0 and γ are the resonant frequency and the linewidth, respectively, and β represents the oscillator strength of the transition. Assuming that the second resonant term is much smaller than the first background term, then $n(\omega)$ can be approximated as

$$n(\omega) = n_\infty + \Delta n(\omega) \quad , \tag{6.a}$$

where

$$n_\infty = \sqrt{\varepsilon_\infty} \quad , \tag{6.b}$$

$$\Delta n(\omega) = \frac{\pi\beta\omega_0}{\sqrt{\varepsilon_\infty}} \frac{1}{\omega_0 - \omega - i\gamma} \quad . \tag{6.c}$$

Once the dispersion relation is obtained, G can be completely expressed by using this form. For transmission measurement, $G(\omega)$ must be given by the wave propagation phenomena, thus

$$\widetilde{G_T}(\omega) = e^{ik(\omega)d} = e^{i\frac{\omega d}{c} n(\omega)} \quad , \tag{7}$$

where d is the sample thickness, and we neglect the phase shift at the surfaces. This approximation should be valid for the weak resonant case. By substituting Eqs. 6.a-b into Eq. 7, one obtains

$$\begin{aligned} \widetilde{G_T}(\omega) &= e^{i\frac{\omega d}{c} n_\infty} e^{i\frac{\omega d}{c} \Delta n(\omega)} \\ &\approx e^{i\frac{\omega d}{c} n_\infty} \left(1 + i\frac{\omega d}{c} \Delta n(\omega)\right) \quad . \end{aligned} \tag{8}$$

By omitting the nonresonant Fabry-Perot contribution, $e^{i\frac{\omega d}{c}n_\infty}$, we obtain

$$G_T(\tau) = \delta(\tau) - \frac{\pi\beta\,\omega_0^2 d}{n_\infty\, c}\,\theta(\tau)\exp[(-i\omega_0 - \gamma/2)\,\tau] \quad , \tag{9}$$

where $\theta(\tau)$ is a step function. The real temporal shape is expressed as time-convolution of Eq. 9. Consequently, the temporal profile of transmitted pulses should show the decay feature of dephasing process. It should be noted that the second term in Eq. 9 has a opposite sign to the first term. This cancellation leads to the macroscopic absorption, which originates from a destructive interference of incident light and the induced coherently emitting light in this treatment.

For reflectance configuration with p-polarized beam, $G(\omega)$ is given by the well-known Fresnel's formula, as

$$\widetilde{G_{R,\theta}}(\omega) = \frac{n(\omega)^2\cos\theta - \sqrt{n(\omega)^2 - \sin^2\theta}}{n(\omega)^2\cos\theta + \sqrt{n(\omega)^2 - \sin^2\theta}} \quad , \tag{10}$$

where θ is the incident angle. In usual experiments we use the normal incident configuration. In that case, $G(\omega)$ simply reduces to,

$$\widetilde{G_{R\perp}}(\omega) = \frac{1 - n(\omega)}{1 + n(\omega)}$$

$$\approx \frac{1 - n_\infty}{1 + n_\infty}\left(1 + \frac{2}{n_\infty^2 - 1}\Delta n(\omega)\right) \quad . \tag{11}$$

The corresponding $G(\tau)$ is given by

$$G_{R\perp}(\tau) = \frac{1 - n_\infty}{1 + n_\infty}\{\,\delta(\tau) + i\,\frac{2\pi\beta\,\omega_0}{n_\infty(n_\infty^2 - 1)}\,\theta(\tau)\exp[(-i\omega_0 - \gamma/2)\,\tau]\,\} \quad . \tag{12}$$

Therefore, Eq. 12 shows that the coherent emission process is seen even in the reflected pulse at normal incidence. Contrary to the transmitting case, the induced coherent light does not interfere with the nonresonant light, since the corresponding two terms are

perpendicular to each other. Also, the ratio of the nonresonant component and the induced one is much smaller than that the transmitting pulse, as

$$\frac{\alpha_T}{\alpha_{R\perp}} = \frac{\omega d / c}{2 / \left(n_\infty^2 - 1\right)} >> 1 \qquad (13)$$

If we adopt the Brewster-angle of incidence configuration for the reflectance measurement, the nonresonant contribution is completely reduced. In this case the incident angle is taken as a Brewster-angle defined as nonresonant region, i.e.,

$$\theta_B = \arctan[n_\infty] \quad . \qquad (14)$$

Then, one finds

$$\widetilde{G_{R,\,\theta_B}}(\omega) \approx \frac{n_\infty^2 - 1}{2n_\infty^3} \Delta n(\omega)$$

and (15)

$$G_{R\theta_B}(\tau) = i \frac{(n_\infty^2 - 1)\, \pi\beta\, \omega_0}{2n_\infty^4} \theta(\tau) \exp[(-i\omega_0 - \gamma/2)\, \tau] \quad . \qquad (16)$$

Thus, the reflected pulse at Brewster angle of incidence displays only the coherent emitting signal free from the nonresonant contribution.

Appendix. B Temporal profile of four-wave-mixing signals

B-1. FWM in noninteracting two-level systems

We examine theoretically the behavior of FWM signal in a noninteracting two-level atomic system, which was first analyzed by Yajima and Taira.[31] In density matrix formalism, the development of the system obeys the Liouville equation, (h = 1)

$$i\frac{\partial}{\partial t}\hat{\varrho} = \left[\hat{H}, \hat{\varrho}\right] \quad , \qquad [1]$$

and the expectation value of the observable is given by

$$\langle\hat{A}\rangle = \text{trace}\left[\hat{A}\hat{\varrho}\right] \quad . \qquad [2]$$

If the interacting light is resonant with one pair of electronic levels, it is sufficient to look only at the motion of these two levels, then the density matrix can be reduced to 2x2 blocks as

$$\hat{\varrho} = \begin{pmatrix} n_e & \phi \\ \phi^* & 1\text{-}n_e \end{pmatrix} \quad , \qquad [3]$$

where n_e and ϕ represent the population of the excited states, and the magnitude of coherent superposition of two states, respectively. The coherent polarization P is written by using ϕ as

$$P = N\mu^*\phi + c.c. \quad , \qquad [4]$$

where N is the volume density of the dipole. The Hamiltonian is given by

$$\hat{H} = \hat{H_0} + \widehat{H_{int}} + \widehat{H_{relax}} \quad , \qquad [5.a]$$

$$\hat{H_0} = \begin{pmatrix} \varepsilon_e & 0 \\ 0 & \varepsilon_g \end{pmatrix} \quad , \qquad [5.b]$$

$$\widehat{H_{int}} = \begin{pmatrix} 0 & -\mu E \\ -u^*E^* & 0 \end{pmatrix} \quad , \qquad [5.c]$$

where $\varepsilon_{e,g}$ are the eigen energies of the excited and ground states, μ, the electric dipole matrix element of the transition, and, E, the applied electric field. H_{relax} describes the coupling to the thermal reservoir and hence the relaxation. For the purpose of the present discussion, we approximate this term by phenomenological transverse and longitudinal relaxation rates $\gamma_2=T_2^{-1}$ and $\gamma_1=T_1^{-1}$, respectively. The temporal evolution of ϕ and n_e is then given respectively by

$$\left(\frac{\partial}{\partial t} + \gamma_2 + i\Omega_0\right)\phi = iV\,(1-2n_e) \quad , \qquad [6.a]$$

$$\left(\frac{\partial}{\partial t} + \gamma_1\right)n_e = i\left[V\phi^* - V^*\phi\right] \quad , \qquad [6.b]$$

where $V = \mu E$ is the Rabi frequency which describes the coupling of the system to the light field, and $\Omega_o = \varepsilon_e - \varepsilon_g$. Eqs. 6.a,b is known as optical Bloch equations. Nonlinear optical process is obtained by the perturbation treatment of the equations. Up to third order perturbation, in which the driving term in the equations is proportional to the third power of electric field, one finds

$$\left(\frac{\partial}{\partial t} + \gamma_2 + i\Omega_0\right)\phi^{(1)} = iV \quad , \qquad [7.a]$$

$$\left(\frac{\partial}{\partial t} + \gamma_1\right)n_e^{(2)} = i\left[V\phi^{(1)*} - V^*\phi^{(1)}\right] \quad , \qquad [7.b]$$

$$\left(\frac{\partial}{\partial t} + \gamma_2 + i\Omega_0\right)\phi^{(3)} = -i2Vn_e^{(2)} \quad . \qquad [7.c]$$

In self-diffracted FWM geometry, two light beams of the wave vectors, k_1 and k_2 with the same frequency ω are incident on the sample, i.e.,

$$E= E_1(t)\,exp[i(k_1r - \omega t)] + E_2(t)\,exp[i(k_2r - \omega t)] \quad . \qquad [8.a]$$

Here we can treat $E(t)$ as an δ-function, i. e.,

$$E_1(t) = E_1\,\delta(t) \quad , \qquad E_2(t) = E_2\,\delta(t - \tau) \quad , \qquad [8.b]$$

where τ represents the time delay between two pulses, and the first pulse arrives at t = 0. By substituting Eqs. 8 into Eqs. 7, we have

$$\phi^{(1)} = i\theta_1\,exp(-\gamma_2 t)\,exp[\,i\,(k_1r - \Omega_0 t)] \quad , \qquad [9.a]$$

$$n_e^{(2)} = \theta_1\theta_2\, exp[(i\Omega_0-\gamma_2)t]\, exp[i(-k_1+k_2)r]\, exp[-\gamma_1(t-\tau)]\, \Theta(t-\tau) + c.c. \quad , \qquad [9.b]$$

$$\phi^{(3)} = -i\,2\,\theta_1\theta_2^2\, exp(-\gamma_2 t)\, exp[i\,(-k_1+2k_2)r]\, exp[-i\Omega_0(t-2\tau)]\, \Theta(t-\tau) \quad , \qquad [9.c]$$

where $\theta_j = \int_{-\infty}^{\infty} d\tau\, \mu E_j(\tau)$ represents so-called pulse area. Eq. 9.b shows the population grating, i. e., the spatial periodic modulation of the excitation.

Consequently, the emitting polarization of FWM is given by

$$P^{(3)homo} = -i\,2\,N\mu^*\theta_1\theta_2^2\, exp(-\gamma_2 t)\, exp[\,i\,(-k_1+2k_2)r]\, exp[-i\Omega_0(t-2\tau)] + c.c. \quad . \qquad [10]$$

This equation gives the expression for the homogeneous broadened transition system, i. e., all dipoles have the same transition energy Ω_0. However, when the inhomogeneity of the crystal gives rise to the broadening of transition energies, the macroscopic polarization is written as a convolution form of Eq. 10, i. e.,

$$P^{(3)inhomo} = \int_0^{\infty} d\Omega_0\, g(\Omega_0)\, P^{(3)homo} \quad , \qquad [11]$$

where $g(\Omega_0)$ represents the normalized density of transition energies. Then the FWM signal in this case is given by

$$P^{(3)inhomo} = -i\,2\,N\mu^*\theta_1\theta_2^2\, exp(-\gamma_2 t)\, exp[\,i\,(-k_1+2k_2)r]\, G(t-2\tau) \quad , \qquad [12]$$

where

$$G(\eta) = \int_0^{\infty} d\Omega_0\, g(\Omega_0)\, exp(-i\Omega_0\eta) \quad . \qquad [13]$$

Eq. 12 shows that although the destructive interference between different oscillating dipoles causes rapid decay of macroscopic polarization, the polarization is recovered through FWM process. This interesting feature is known as photon echo, where a pulse-like emission signal, $G(\tau)$, is observed at around $t = 2\tau$.

B-2. FWM in highly excited semiconductors

Recently it has been pointed out that the applicability of two-level model to Wannier excitons can be limited, since exciton is a collective excitation with finite extent. One theoretical approach is based on the Hartree-Fock approximations of Coulomb interactions.[16, 19] This theory successfully describes the coherent excitonic transients in highly-densed III-V compound semiconductors. In this section we derive the FWM signal expected in this theory.

We consider a parabolic two-band model with the conduction band c and valence band v. Neglecting the photon momentum, the optically coupled conduction and valence band states form a set of two-level system labeled by wave vectors k. The density matrix of the semiconductor is expressed as,

$$\widehat{\varrho_v(t)} = \begin{pmatrix} n_{ck}(t) & \phi_k(t) \\ \phi_k^*(t) & n_{vk}(t) \end{pmatrix}, \tag{1}$$

where $n_{c,\,vk}$ are the respective populations in the conduction and valence bands (at thermal equilibrium, $n_c = 0$ and $n_v = 1$), and ϕ_k is the electron-hole (e-h) pair amplitude. The induced total polarization (per spin degree of freedom) is

$$P = \sum_k \mu^* \phi_k(t) + c.c. \quad . \tag{2}$$

The density matrix obeys the Liouville equation ($h = 1$),

$$\frac{\partial}{\partial t}\widehat{\varrho_k} = -i\left[\widehat{H_k}, \widehat{\varrho_k}\right] + \frac{\partial}{\partial t}\widehat{\varrho_k}\Big|_{\text{relax}} \quad . \tag{3}$$

The difference of this model from noninteracting two level system is that the Coulomb interaction $V_{k,\,k'}$ couples the various states. In the presence of strong field E, the Hamiltonian is

$$\widehat{H_k} = \begin{pmatrix} \varepsilon_{ck}^0 & -\mu E \\ -\mu^* E^* & \varepsilon_{vk}^0 \end{pmatrix} - \sum_{k'} V_{k,\,k'}\,\widehat{\varrho_{k'}} \quad , \tag{4}$$

where μE is the effective Rabi frequency. The unperturbed conduction and valence band energies are $\varepsilon_{ck}^0 = E_g/2 + \mathbf{k}^2/2m_e$ and $\varepsilon_{vk}^0 = -E_g/2 - \mathbf{k}^2/2m_h + \Sigma_{k'} V_{k,k'}$, where E_g is

the band gap. As compared to noninteracting two-level systems, the physics is modified by the Coulomb force in two ways: (i) the energies are renormalized,

$$\varepsilon_{jk}^{0} \rightarrow \varepsilon_{jk}(t) = \varepsilon_{ck}^{0} - \sum_{k'} V_{k,k'}\ n_{jk'}(t)\ , \quad j = c, v \tag{5.a}$$

and (ii) the coupling to the light is modified according to

$$\mu E(t) \rightarrow \Delta_k(t) = \mu E(t) + \sum_{k'} V_{k,k'}\ \phi_{k'}(t)\ , \tag{5.b}$$

This modification describes the fact that the e-h states do not only experience the applied field μE; rather they see the self consistent "local field" Δ_k, which is the sum of the applied field and the "self-induced" field due to all the other e-h states at different wave vectors $\mathbf{k}'$. As a result, the temporal evolution of the e-h pair amplitude and the population is given by

$$\left(\frac{\partial}{\partial t} + \gamma_2 + i\left[\varepsilon_{ck}(t) - \varepsilon_{vk}(t)\right]\right)\phi_k(t) = i\Delta_k(t)\left(1\text{-}2n_k(t)\right) \quad , \tag{6.a}$$

$$\left(\frac{\partial}{\partial t} + \gamma_1\right) n_k(t) = i\left[\Delta_k(t)\phi_k^{*}(t) - \Delta_k(t)^{*}\phi_k(t)\right] \quad , \tag{6.b}$$

where we have used the e-h pair representation $n_{ck} \rightarrow n_k$ and $n_{vk} \rightarrow 1 - n_k$. This expression is known as semiconductor Bloch equation. The linear response provided by using this expression shows the same form with the usual Wannier equation for excitons. Also, it is noted that by setting the Coulomb interaction $V_{\mathbf{k},\mathbf{k}'}$ equal to zero, the above set of equations reduces to the usual Bloch equations for noninteracting two level model.

In order to see the role of "local field effects" induced by Coulomb interaction term, we consider an idealized model which contains all the important physics. The transition amplitude y and excited state population n satisfy the modified Bloch equation, in which the driving terms involve not only the applied field, but Lorentz local field,

$$\left[\frac{\partial}{\partial t} + \gamma_2 + i\,\Omega_0\right]\psi(t) = i\left[1 - 2n(t)\right]\Delta(t) \quad , \tag{7.a}$$

$$\left[\frac{\partial}{\partial t} + \gamma_1\right] n(t) = -2\mathrm{Im}\left[i\,\psi(t)\Delta(t)^{*}\right] \quad , \tag{7.b}$$

where Ω_0 is the transition energy and

$$\Delta(t) = \mu E(t) + V\psi(t) \qquad (8)$$

These equations have the same structure as Eqs. 6, except neglecting the momentum dependence of y and n, and self-energy correction term. In linear response one finds that Coulomb interaction V merely renormalizes the transition energy to $\Omega = \Omega_0 - V$. This means V gives the exciton binding energy in this treatment. The form of $\Delta(t)$ indicates that the driving term still continues in T_2 after the incidence of a pulse. This is the crucial difference between a noninteracting and an interacting set of two levels atoms.

The perturbation treatment is similar to that without local-field corrections. Up to third order, one finds

$$\left[\frac{\partial}{\partial t} + \gamma_2 + i\,\Omega\right] \psi^{(1)}(t) = i\ F(t) \quad , \qquad (9.a)$$

$$\left[\frac{\partial}{\partial t} + \gamma_1\right] n^{(2)}(t) = i\left[\psi^{(1)}(t)F(t)^* - \psi^{(1)}(t)^*F(t)\right] \quad , \qquad (9.b)$$

and

$$\left[\frac{\partial}{\partial t} + \gamma_2 + i\,\Omega\right] \psi^{(3)}(t) = -i2\, n^{(2)}(t)\ \left[F(t) + V\psi^{(1)}(t)\right] \quad . \qquad (9.c)$$

For the self-diffracted FWM situation, i.e., $E = E_1\delta(t)\ \exp[i(k_1 r - \omega t)] + E_2\delta(t - \tau)\ \exp[i(k_2 r - \omega t)]$, the solution of Eqs. 9 yields for a homogeneously broadened system

$$\begin{aligned}\psi^{(3)} = -i2\theta_1\theta_2^2 \exp[\, i(-k_1 + 2k_2)r]\, \exp[\, -i\Omega(t - 2\tau) - \gamma_2 t] \\ \{\, \Theta(\tau)\, \Theta(t - \tau) \\ + \Theta(\tau)\, \Theta(t - \tau)\, i2V\, (t - \tau) \\ + \Theta(-\tau)\, \Theta(t)\, i2Vt \exp[2\gamma_2\tau]\, \}\end{aligned} \qquad (10)$$

where $\theta_j = \int_{-\infty}^{\infty} d\tau\, \mu E_j(\tau)$ and Θ is the step function. Eq. 10 comprises three terms. The first one is the usual term for noninteracting two-level model. The two other terms proportional to V are due to the local field correction. The first term shows the enhancement of usual two-level signal whereas the other (proportional to $\Theta(\tau)$) contributes only for negative time delay. Since the these terms are orthogonal, this three contributions do not interfere to each other.

It was reported that FWM emission at negative time-delay was experimentally observed for a GaAs MQWs, as expected in this theory.[17, 18] However, the limitation on the usage of semiconductor Bloch equation has been also pointed out. Problems are typically seen in that the excitonic many-body interaction in this treatment provides only the growth of coherence; phase relaxation caused by exciton-exciton scattering is completely ignored. This treatment is only applicable to the system where exciton is dissociated, such as high densed situation in which Coulomb force is enough small by screening, or at semiconductors with small exciton binding energy like GaAs (3 meV). It should be necessary to build a new theoretical expression where the unperturved state is exciton, but e-h pair, then it would describes the coherent transients even in low exciton densities.

Appendix C. Temporal profile of FWM in the case of PI and QB

We examine theoretically the temporal profile of FWM signal in the case of PI and QB. In density matrix formalism, the development of the system obeys the Liouville equation, ($\hbar = 1$)

$$i\frac{\partial}{\partial t}\hat{\varrho} = \left[\hat{H}, \hat{\varrho}\right] \quad . \qquad [1]$$

First we consider the situation for realizing QB, where two closely-separated excited states have a common ground state. Since, the system can be described as a three-level system, the density matrix becomes 3 x 3 blocks

$$\hat{\varrho} = \begin{pmatrix} n_2 & \psi & \phi_2 \\ \psi^* & n_1 & \phi_1 \\ \phi^*_2 & \phi^*_1 & n_g \end{pmatrix} , \qquad [2]$$

where n_g, n_1, and n_2 are the populations of the ground, first and second excited states, ϕ_i denotes the coherent superposition of i-th excited and ground states, and ψ represents the magnitude of the sublevel coherence. The macroscopic polarization P is given by

$$P(t) = \mu_1\phi_1(t) + \mu_2\phi_2(t) \quad , \qquad [3]$$

where μ_i is the dipole matrix element of the transition between the ground and i-th excited state. The observed intensity of emitted light is given as

$$I(t) \propto |P(t)|^2 \quad . \qquad [4]$$

The Hamiltonian of the system is given by

$$\hat{H} = \hat{H}_0 + \hat{H}_{int} + \hat{H}_{relax} \qquad \text{with} \qquad [5.a]$$

$$\hat{H}_0 = \begin{pmatrix} \Omega_2 & & \\ & \Omega_1 & \\ & & 0 \end{pmatrix} , \text{ and } \hat{H}_{int} = \begin{pmatrix} & & -\mu_2 E \\ & & -\mu_1 E \\ -\mu^*_2 E^* & -\mu^*_1 E^* & 0 \end{pmatrix} \quad , \qquad [5.b]$$

where Ω_i is the i-th transition energy and E is the applied electric field. H_{relax} describes the coupling to the thermal reservoir. For the purpose of the present discussion, we

approximate this term by phenomenological transverse and longitudinal relaxation rate γ_i and Γ_i, respectively. The temporal evolution of the density matrix element is then given by

$$\left[\frac{\partial}{\partial t} + \gamma_1 + i\Omega_1\right]\phi_1(t) = i\left[\left(1 - 2n_1 - n_2\right)\mu_1 E - \psi^* \mu_2 E\right] \quad , \qquad [6.a]$$

$$\left[\frac{\partial}{\partial t} + \gamma_2 + i\Omega_2\right]\phi_2(t) = i\left[\left(1 - n_1 - 2n_2\right)\mu_2 E - \psi\, \mu_1 E\right] \quad , \qquad [6.b]$$

$$\left[\frac{\partial}{\partial t} + \gamma_{12} + i(\Omega_2 - \Omega_1)\right]\psi(t) = i\left[\phi^*_1 \mu_2 E - \phi_2 \mu^*_1 E^*\right] \quad , \qquad [6.c]$$

where $\Omega_d = \Omega_2 - \Omega_1$, and

$$\left[\frac{\partial}{\partial t} + \Gamma_1\right]n_1(t) = i\left[\phi^*_1 \mu_1 E - \phi_1 \mu^*_1 E^*\right] \quad , \qquad [6.d]$$

$$\left[\frac{\partial}{\partial t} + \Gamma_2\right]n_2(t) = i\left[\phi^*_2 \mu_2 E - \phi_2 \mu^*_2 E^*\right] \quad . \qquad [6.e]$$

Nonlinear optical process is described by the perturbation treatment of the equations. FWM is given by the third order nonlinear polarization. Up to third order perturbation, in which the driving term in the equations is proportional to the third power of electronic fields, one finds

$$\left[\frac{\partial}{\partial t} + \gamma_1 + i\Omega_1\right]\phi_1^{(1)}(t) = i\,\mu_1 E \quad , \qquad [7.a]$$

$$\left[\frac{\partial}{\partial t} + \gamma_2 + i\Omega_2\right]\phi_2^{(1)}(t) = i\,\mu_2 E \quad , \qquad [7.b]$$

$$\left[\frac{\partial}{\partial t} + \Gamma_1\right]n_1^{(2)}(t) = i\left[\phi^{*(1)}_1 \mu_1 E - \phi_1^{(1)} \mu^*_1 E^*\right] \quad , \qquad [7.c]$$

$$\left[\frac{\partial}{\partial t} + \Gamma_2\right] n_2^{(2)}(t) = i\left[\phi^*{}_2^{(1)}\,\mu_2 E - \phi_2^{(1)}\,\mu^*{}_2 E^*\right] \quad , \qquad [7.d]$$

$$\left[\frac{\partial}{\partial t} + \gamma_{12} + i(\Omega_2 - \Omega_1)\right] \psi^{(2)}(t) = i\left[\phi^*{}_1^{(1)}\,\mu_2 E - \phi_2^{(1)}\,\mu^*{}_1 E^*\right] \quad , \qquad [7.e]$$

$$\left[\frac{\partial}{\partial t} + \gamma_1 + i\Omega_1\right] \phi_1^{(3)}(t) = i\left[\left(-2n_1^{(2)} - n_2^{(2)}\right)\mu_1 E - \psi^{(2)*}\,\mu_2 E\right] \quad , \qquad [7.f]$$

$$\left[\frac{\partial}{\partial t} + \gamma_2 + i\Omega_2\right] \phi_2^{(3)}(t) = i\left[\left(-n_1^{(2)} - 2n_2^{(2)}\right)\mu_2 E - \psi^{(2)}\,\mu_1 E\right] \quad . \qquad [7.g]$$

We observe the so-called self-diffracted FWM signals, where two light beams of the wave vectors, $\boldsymbol{k}_1$ and $\boldsymbol{k}_2$ with the same frequency ω are incident on the sample, with emitting FWM signal in the direction of $-\boldsymbol{k}_1 + 2\boldsymbol{k}_2$, then

$$E = E_1(t)\exp[i(\boldsymbol{k}_1 \cdot \mathbf{r} - \omega t)] + E_2(t)\exp[i(\boldsymbol{k}_2 \cdot \mathbf{r} - \omega t)] \quad . \qquad [8]$$

For simplicity, we can approximate that the incident pulse is short enough to be taken by a δ function

$$E_1(t) = E_1\,\delta(t), \quad E_2(t) = E_2\,\delta(t - \tau) \quad , \qquad [9]$$

where the first pulse arrives at $t = 0$, and the second pulse is delayed by τ. The observed FWM signal is given by picking up the term which is linear to $\exp[i(-\boldsymbol{k}_1 + 2\boldsymbol{k}_2)\cdot \boldsymbol{r}]$ from the third order polarization, then

$$P_{QB}^{(3)} = \mu_1 A\,F(\tau)\,f(t) \quad , \qquad [10.a]$$

where

$$A = -2\,i\,N\,e^{-i(-\boldsymbol{k}_1 + 2\boldsymbol{k}_2)\cdot \boldsymbol{r}}\,\theta_1\theta_2^2 \quad , \qquad [10.b]$$

$$F(\tau) = e^{(i\Omega_1 - \gamma_1)\tau} + c^2\,e^{(i\Omega_2 - \gamma_2)\tau} \quad , \qquad [10.c]$$

$$f(t) = \left[e^{(-i\Omega_1 - \gamma_1)(t - \tau)} + c^2\,e^{(-i\Omega_2 - \gamma_2)(t - \tau)}\right]\Theta(t - \tau) \quad . \qquad [10.d]$$

where N is the density of the dipole, and

$$\theta_j = \int_{-\infty}^{\infty} dt\ \mu_1 E_j(t) \quad , \qquad [11]$$

denotes the pulse area applied by the j-th pulse for the transition related to the first excited states, c = μ_1/μ_2 , and Θ, the step function. To derive Eqs. 10.a-d, we substitute Eqs. 8 and 9 into Eqs. 7 and 3.

For the situation for PI, the FWM signal is simply given by the superposition of two two-level-type nonlinear polarization with the different energy of Ω_1 and Ω_2. (see Appendix B) The temporal development for PI is then give by

$$P_{PI}^{(3)} = \mu_1 A\, g(t) \quad , \qquad [12]$$

$$g(t) = e^{-\gamma t}\left[w_1\, e^{-i\Omega_1 (t\,-\,2\tau)} + w_2\, e^{-i\Omega_2 (t\,-\,2\tau)}\right] \quad , \qquad [13]$$

where w_1 shows the weight for the dipole of the energy Ω_1.

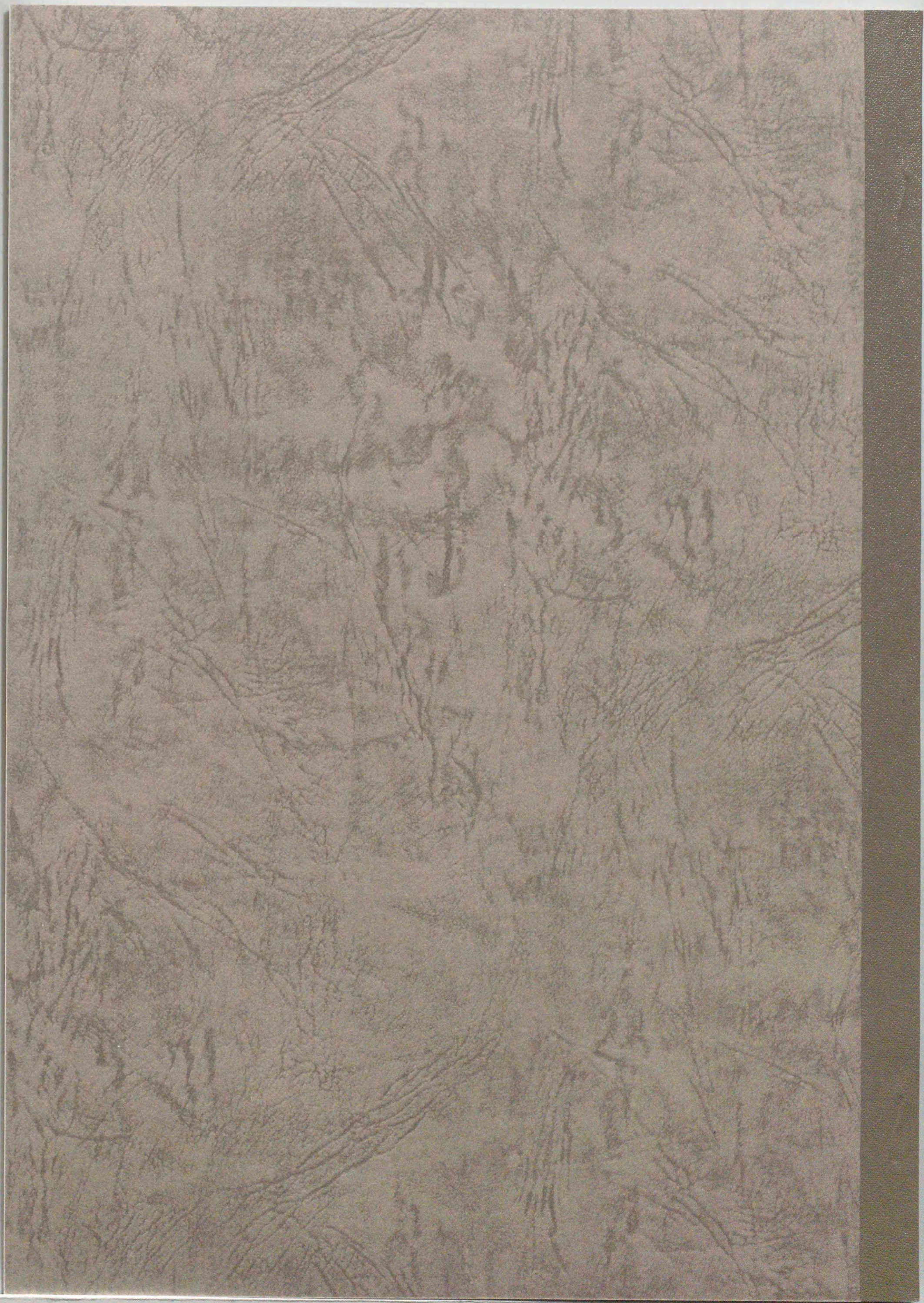

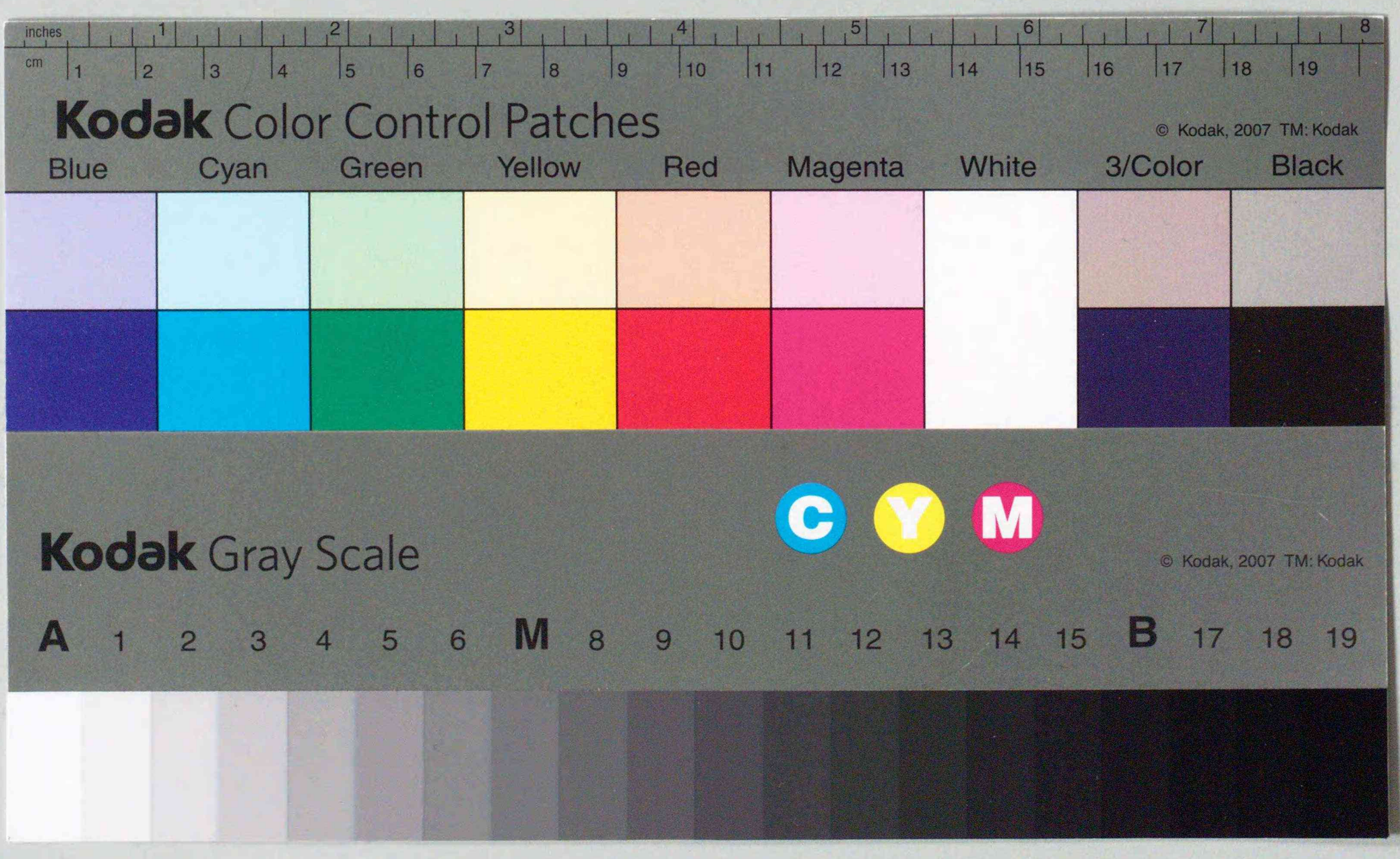
inches
cm
Kodak Color Control Patches
© Kodak, 2007 TM: Kodak
Blue
Cyan
Green
Yellow
Red
Magenta
White
3/Color
Black
Kodak Gray Scale
C
Y
M
© Kodak, 2007 TM: Kodak
A 1 2 3 4 5 6 M 8 9 10 11 12 13 14 15 B 17 18 19